Check for updates
NANO · MICRO small
www.small-journal.com

Toward Unusual-High Hole Mobility of p-Channel Field-Effect-Transistors

Jiamin Sun, Xinming Zhuang, Yibo Fan, Shuai Guo, Zichao Cheng, Dong Liu, Yanxue Yin, Yufeng Tian, Zhiyong Pang, Zhipeng Wei, Xiufeng Song, Lei Liao, Feng Chen, Johnny C. Ho,* and Zai-xing Yang**

The relative low hole mobility of p-channel building block device challenges the continued miniaturization of modern electronic chips. Metal-semiconductor junction is always an efficient strategy to control the carrier concentration of channel semiconductor, benefiting the carrier mobility regulation of building block device. In this work, complementary metal oxide semiconductor (CMOS)-compatible metals are selected to deposit on the surface of the important p-channel building block of GaSb nanowire field-effect-transistors (NWFETs), demonstrating the efficient strategy of hole mobility enhancement by metal-semiconductor junction. When deposited with lower work function metal of Al, the peak hole mobility of GaSb NWFET can be enhanced to as high as ≈3372 $cm^2 V^{-1} s^{-1}$, showing three times than the un-deposited one. The as-studied metal-semiconductor junction is also efficient for the hole mobility enhancement of other p-channel devices, such as GaAs NWFET, GaAs film FET, and WSe_2 FET. With the enhanced mobility, the as-constructed CMOS inverter shows good invert characteristics, showing a relatively high gain of ≈18.1. All results may be regarded as important advances to the next-generation electronics.

1. Introduction

In modern electronic chips, the carrier mobility of p-channel building block devices always shows lower value than n-channel ones, challenging their continued miniaturization in electronics and optoelectronics.[1–3] The carrier mobility of the as-mentioned building block devices depends mainly on the device fabrication technology and the channel semiconductors. The fabrication technology is complex and each of the processes is crucial to the carrier mobility of the as-fabricated building block devices. For example, Park et al. pointed out that the peak electron mobility of graphene field-effect-transistors (FETs) can be improved up to four times by using a cleaner substrate during the device fabrication process.[4] On the other hand, the carrier mobility of the as-mentioned building block devices can be regulated by the crystallinity, growth plane, carrier effective mass, carrier concentration, etc. of channel semiconductors. With a better crystallinity, InGaZnO nanowires (NWs)-,[5] β-Ga_2O_3 nanosheets-,[6] and black phosphorus film-based FETs[7] have shown the enhanced mobilities in the kinds of literature, owing to the decreased transport scattering. Meanwhile, with a designed crystal growth plane, the polarity, carrier effective mass, and surface scattering of InP NWs,[8] layered $PtSe_2$,[9] and multilayer InSe[10] can be controlled, resulting in the higher mobilities of FETs.

J. M. Sun, X. M. Zhuang, Y. B. Fan, D. Liu, Y. X. Yin, Y. F. Tian, Z. Y. Pang, F. Chen, Z.-x. Yang
School of Physics
School of Microelectronics
State Key Laboratory of Crystal Materials
Shandong University
Jinan 250100, P. R. China
E-mail: zaixyang@sdu.edu.cn

J. M. Sun, D. Liu, Z.-x. Yang
State Key Laboratory of Infrared Physics
Shanghai Institute of Technical Physics
Chinese Academy of Sciences
Shanghai 200083, P. R. China

S. Guo, Z. P. Wei
State Key Laboratory of High Power Semiconductor Lasers
Changchun University of Science and Technology
Changchun 130022, P. R. China

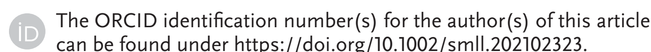
The ORCID identification number(s) for the author(s) of this article can be found under https://doi.org/10.1002/smll.202102323.

DOI: 10.1002/smll.202102323

Z. C. Cheng, X. F. Song
Institute of Optoelectronics and Nanomaterials
MIIT Key Laboratory of Advanced Display Materials and Devices
College of Materials Science and Engineering
Nanjing University of Science and Technology
Nanjing 210094, China

L. Liao
Key Laboratory for Micro-Nano Optoelectronic Devices of Ministry of Education
School of Physics and Electronics
Hunan University
Changsha 410082, P. R. China
E-mail: liaolei@hnu.edu.cn

J. C. Ho
Department of Materials Science and Engineering
City University of Hong Kong
Hong Kong 999077, P. R. China
E-mail: johnnyho@cityu.edu.hk

© 2021 Wiley-VCH GmbH

NANO · MICRO small
www.small-journal.com

Toward Unusual-High Hole Mobility of p-Channel Field-Effect-Transistors

Jiamin Sun, Xinming Zhuang, Yibo Fan, Shuai Guo, Zichao Cheng, Dong Liu, Yanxue Yin, Yufeng Tian, Zhiyong Pang, Zhipeng Wei, Xiufeng Song, Lei Liao, Feng Chen, Johnny C. Ho,* and Zai-xing Yang**

The relative low hole mobility of p-channel building block device challenges the continued miniaturization of modern electronic chips. Metal-semiconductor junction is always an efficient strategy to control the carrier concentration of channel semiconductor, benefiting the carrier mobility regulation of building block device. In this work, complementary metal oxide semiconductor (CMOS)-compatible metals are selected to deposit on the surface of the important p-channel building block of GaSb nanowire field-effect-transistors (NWFETs), demonstrating the efficient strategy of hole mobility enhancement by metal-semiconductor junction. When deposited with lower work function metal of Al, the peak hole mobility of GaSb NWFET can be enhanced to as high as ≈3372 $cm^2\ V^{-1}\ s^{-1}$, showing three times than the un-deposited one. The as-studied metal-semiconductor junction is also efficient for the hole mobility enhancement of other p-channel devices, such as GaAs NWFET, GaAs film FET, and WSe_2 FET. With the enhanced mobility, the as-constructed CMOS inverter shows good invert characteristics, showing a relatively high gain of ≈18.1. All results may be regarded as important advances to the next-generation electronics.

1. Introduction

In modern electronic chips, the carrier mobility of p-channel building block devices always shows lower value than n-channel ones, challenging their continued miniaturization in electronics and optoelectronics.[1–3] The carrier mobility of the as-mentioned building block devices depends mainly on the device fabrication technology and the channel semiconductors. The fabrication technology is complex and each of the processes is crucial to the carrier mobility of the as-fabricated building block devices. For example, Park et al. pointed out that the peak electron mobility of graphene field-effect-transistors (FETs) can be improved up to four times by using a cleaner substrate during the device fabrication process.[4] On the other hand, the carrier mobility of the as-mentioned building block devices can be regulated by the crystallinity, growth plane, carrier effective mass, carrier concentration, etc. of channel semiconductors. With a better crystallinity, InGaZnO nanowires (NWs)-,[5] β-Ga_2O_3 nanosheets-,[6] and black phosphorus film-based FETs[7] have shown the enhanced mobilities in the kinds of literature, owing to the decreased transport scattering. Meanwhile, with a designed crystal growth plane, the polarity, carrier effective mass, and surface scattering of InP NWs,[8] layered $PtSe_2$,[9] and multilayer InSe[10] can be controlled, resulting in the higher mobilities of FETs.

J. M. Sun, X. M. Zhuang, Y. B. Fan, D. Liu, Y. X. Yin, Y. F. Tian, Z. Y. Pang, F. Chen, Z.-x. Yang
School of Physics
School of Microelectronics
State Key Laboratory of Crystal Materials
Shandong University
Jinan 250100, P. R. China
E-mail: zaixyang@sdu.edu.cn

J. M. Sun, D. Liu, Z.-x. Yang
State Key Laboratory of Infrared Physics
Shanghai Institute of Technical Physics
Chinese Academy of Sciences
Shanghai 200083, P. R. China

S. Guo, Z. P. Wei
State Key Laboratory of High Power Semiconductor Lasers
Changchun University of Science and Technology
Changchun 130022, P. R. China

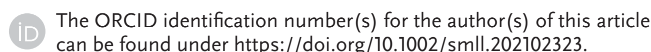
The ORCID identification number(s) for the author(s) of this article can be found under https://doi.org/10.1002/smll.202102323.

DOI: 10.1002/smll.202102323

Z. C. Cheng, X. F. Song
Institute of Optoelectronics and Nanomaterials
MIIT Key Laboratory of Advanced Display Materials and Devices
College of Materials Science and Engineering
Nanjing University of Science and Technology
Nanjing 210094, China

L. Liao
Key Laboratory for Micro-Nano Optoelectronic Devices of Ministry of Education
School of Physics and Electronics
Hunan University
Changsha 410082, P. R. China
E-mail: liaolei@hnu.edu.cn

J. C. Ho
Department of Materials Science and Engineering
City University of Hong Kong
Hong Kong 999077, P. R. China
E-mail: johnnyho@cityu.edu.hk

 © 2021 Wiley-VCH GmbH

In the past decades, the control on carrier concentration of channel semiconductors has been considered as an efficient way to regulate the carrier mobility of building block devices.[11–12] Doping is the most memorable and useful method to realize the control of carrier concentration.[13–14] Generally speaking, the carrier mobility of intrinsic semiconductors increases with the decrease of carrier concentration.[15] In this case, it should be noticed that the concentration and kinds of the dopant are important, otherwise, the additionally introduced carrier and crystal defects will increase the carrier concentration and transport scattering, resulting in the decrease of carrier mobility.[16] As a result, it is rare to report the carrier concentration decrease and mobility increase of channel semiconductors by doping in the literature. For intrinsic p-type semiconductors, slight doping will help to improve the crystallinity quality and decrease the hole concentration, resulting in the enhanced hole mobility.[16] Beyond doping, the carrier concentration of channel semiconductors also can be controlled by constructing metal-semiconductor junctions in the building block devices.[17–18] When the semiconductors contact with the lower work function metals, the electrons from metal will inject into semiconductors, resulting in the increase of electron concentration in n-type semiconductors or the decrease of hole concentration in p-type semiconductors. On the other hand, the electron concentration will decrease in n-type semiconductors or hole concentration will increase in p-type semiconductors when the semiconductors contact with the higher work function metals. In a word, the electron mobility of the n-channel building block device will increase by contacting with the higher work function metals, otherwise, the hole mobility of the p-channel building block device will increase by contacting with the lower work function metals.[15]

Metal-semiconductor junctions can be realized easily by depositing metal nanoparticles on the surface of the building block device.[19] Although several works have focused on the threshold voltage (V_{TH}) manipulation of the n-channel building block device by metal-semiconductor junctions,[17–18] it is still a lacking of detailed investigation of hole mobility manipulation on p-channel building block device. Furthermore, in the modern electronic chips, complementary metal-oxide semiconductor (CMOS)-compatible metals of Al, Sn, Ti, etc. always have low work functions,[20] benefiting the achievement of high hole mobility p-channel building blocks device. In this work, GaSb NW has been selected as the studied p-channel semiconductor, owing to its highest hole mobility among all III–V group semiconductors and the development of high-performance all-around-gated one-dimensional NWFETs has been considered as an optimal solution for the continuation of Moore's Law in the near future.[16,21,22] When deposited with the low work function metals of Al, Sn, and Ti, the peak hole mobilities of GaSb NWFETs are as high as 3372, 1938, and 2840 cm^2 V^{-1} s^{-1}, respectively. At the same time, the other important electronic properties of GaSb NWFETs, such as V_{TH}, and subthreshold (SS) also manipulated well in expect. Importantly, when connected with n-type InGaAs NWs, the fabricated CMOS invert shows good invert characteristics with a relatively high gain of ≈18.1, benefiting from the enhanced hole mobility, the manipulated V_{TH}, and SS, etc. This hole mobility enhancement strategy is also efficient in other p-channel devices, such as GaAs NWFET, GaAs film FET, and 2D WSe_2 FET. All results confirm the promise of these unusual-high hole mobility FETs obtained by metal-semiconductor junction for a wide range of applications in future technology.

2. Results and Discussion

For achieving unusual-high hole mobility, CMOS-compatible metals with different low work functions are adopted here for constructing metal-semiconductor junctions to demonstrate the hole mobility regulation of p-channel GaSb NWFETs. As shown in **Figure 1**, unusual-high hole mobility of GaSb NWFETs are achieved by constructing Al-GaSb junctions. Figure 1a illustrates the typical atomic force microscopy image of GaSb NWFET after the deposition of 0.5 nm Al film, displaying the uniform dispersion of metal nanoparticles on the surface of NWFET. The NW length in the channel is around 3 µm and the diameter is around 30 nm. Figure 1b shows the transfer characteristics in linear coordinates of the GaSb NWFET before and after the deposition of 0.5 nm Al film. Obviously, the deposition of Al film can effectively shift V_{TH} negatively, from 6.8 to 1.5 V. The lower V_{TH} illustrates the easier regulation of FETs under low gate voltage. At the same time, FETs remain ohmic contact after the construction of Al-GaSb junctions, which can be proved by the output characteristics of Figure S1a, Supporting Information. To study the thickness effect of deposition metal film, other thicknesses of 0.1, 1, and 2 nm Al films are also deposited on the surfaces of GaSb NWFETs, respectively. As shown in the transfer characteristics of Figure S1b–d, Supporting Information and the statistics of the V_{TH} shift of Figure 1c, it is obvious that the shift value of V_{TH} increases with the thickness increase of Al film. The mean value of V_{TH} shift is -2.1, −5.2, −4.8, and −7.6 V, respectively, by depositing 0.1, 0.5, 1, and 2 nm Al film. Besides the observation of V_{TH} shift, SS showed in Figure S2a, Supporting Information also decrease from 0.32 to 0.13 V dec^{-1} but I_{on}/I_{off} remains of 10^4 orders. Obviously, all these results will benefit the mobility enhancement of GaSb NWFETs.

With the negative shifted V_{TH}, decreased SS, and remained I_{on}/I_{off}, FE hole mobility of GaSb NWFETs increases significantly, as shown in Figure 1d. The peak hole mobility of GaSb NWFET increases from 1214 to 3372 cm^2 V^{-1} s^{-1} after the construction of Al-GaSb junctions. The hole mobility is calculated by using the analytical equation of $\mu = g_m \times (L^2/C_{OX}) \times (1/V_{DS})$, where the transconductance (g_m) can be extracted from the transfer characteristics following the equation of $g_m = (dI_{DS})/(dV_{GS})|V_{DS}$, and C_{OX} is the gate capacitance obtained from the finite element analysis software COMSOL with respect to different NW diameters. With different thicknesses of Al films, the mean value of mobility increase is 24.1, 1607, 1429, and 1437cm^2 V^{-1} s^{-1} respectively, as shown in Figure 1e. The mobility enhancement is unobvious after the deposition of 0.1 nm Al film, which is probably because of the low density of Al nanoparticles on the surface of GaSb NWs. On the other hand, the hole mobility of the FETs deposited with 2 nm Al film shows a little lower value than ones deposited with 0.5 nm Al film. The sizes of Al nanoparticles would be larger in 2 nm Al film than 0.5 nm film, leading to the less efficient carrier injunction channel between

© 2021 Wiley-VCH GmbH

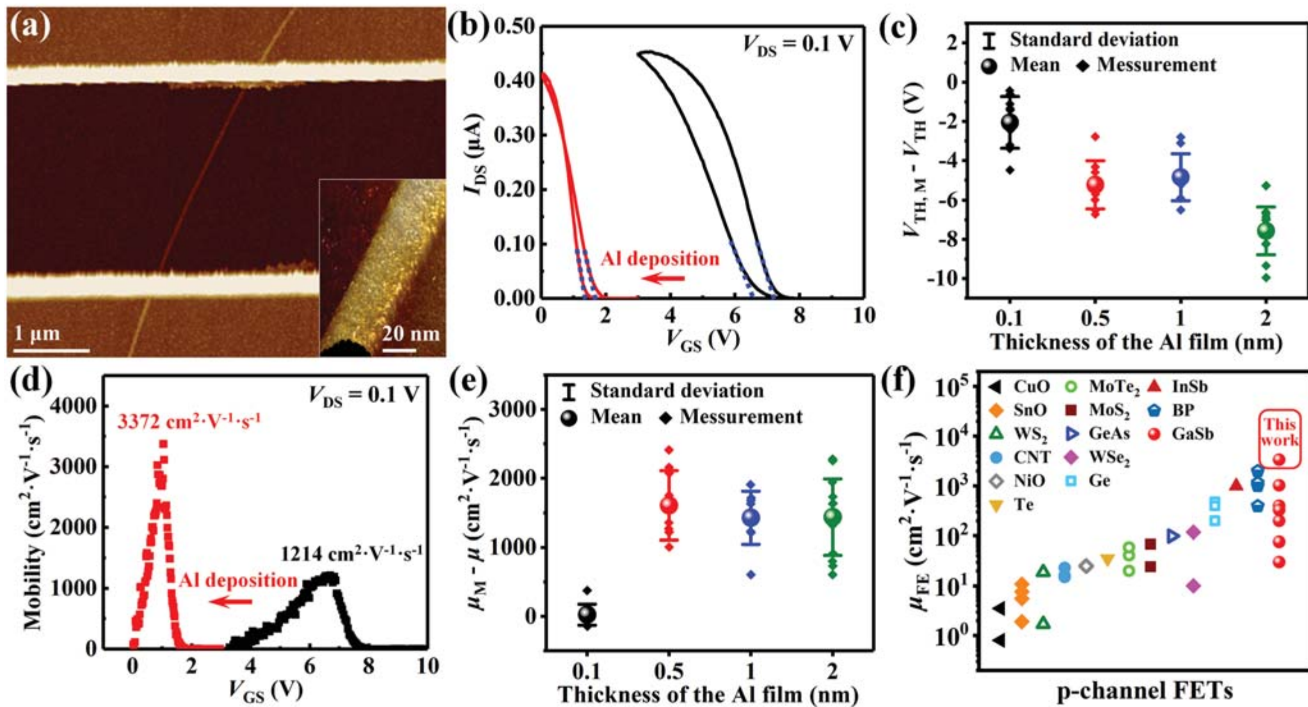

Figure 1. Toward unusual-high hole mobility of GaSb NWFETs by Al-GaSb junctions. a) Typical atomic force microscopy (AFM) image of GaSb NWFET deposited with 0.5 nm Al film. Inset shows the corresponding three-dimensional AFM image of channel GaSb NW; b) transfer characteristics of GaSb NWFET before and after the deposition of Al film; c) V_{TH} shift statistics of GaSb NWFETs deposited with different thicknesses of Al films (V_{DS} = 0.1 V); d) field-effect (FE) mobility of GaSb NWFET before and after depositing 0.5 nm Al film; e) statistics of mobility enhancement of GaSb NWFETs as function of Al film thickness (V_{DS} = 0.1 V); f) FE hole mobilities of typical p-channel (CuO,[23,24] SnO,[25–28] WS_2,[29,30] CNT,[31–33] NiO,[34] Te,[35] $MoTe_2$,[36–38] MoS_2,[39,40] GeAs,[41] WSe_2,[42,43] Ge,[44–46] InSb,[47] BP,[48–51] GaSb[16,21–22,52–54]) FETs in the literatures (at room temperature in the atmosphere).

Al and GaSb. Anyway, this phenomenon is interesting and will be studied in the near future. Especially, the demonstrated unusual-high hole mobility of 3372 $cm^2 V^{-1} s^{-1}$ in this work is the highest room-temperature value among p-channel FETs in the atmosphere in the literature. As shown in Figure 1f, most of the p-channel FETs, such as p-type oxide semiconductor TFTs of CuO,[23,24] SnO,[25–28] NiO,[34] and typical p-type 2D transition-metal dichalcogenides FETs of WS_2,[29,30] $MoTe_2$,[36–38] MoS_2,[39,40] WSe_2,[42,43] exhibit the hole mobilities between the order of 10^0 to 10^2 $cm^2 V^{-1} s^{-1}$. Recently, few-layer black phosphorus (BP)-based FET is also considered as one of the good candidates for p-channel building blocks, as its reported FE hole mobility can reach up to 5200 $cm^2 V^{-1} s^{-1}$.[55] However, the device fabrication and measurement processes require a vacuum environment rather than in the atmosphere, challenging further applications in electronics and optoelectronics. In short, the deposition of low work function metal of Al on the surface of GaSb NWFETs is really an efficient hole mobility enhancement strategy.

To shed light on the mobility regulation mechanism, metal films with different work functions are deposited on GaSb NWFETs to construct metal-semiconductor junctions, along with the systematic investigation of electrical properties. As shown in **Figure 2**a,b, with the deposition of lower work function metals of Ti and Sn (4.33 eV for Ti and 4.42 eV for Sn), V_{TH} of GaSb NWFET shifts negatively, from 6.4 to 1.1 V, and from 6.5 to 0.4 V, respectively. On the contrary, V_{TH} of GaSb NWFET shifts positively, from 6.5 to 8.4 V and from 5.6 to 15.3 V, respectively, when the higher work function metals of Ni (5.04–5.35 eV) and Pt (5.64–5.93 eV) are deposited, as shown in Figure 2c and Figure S4, Supporting Information, which mainly because of the hole concentration increase and require a larger gate voltage to realize the regulation of FETs. As shown in Figure 2d of the statistics of V_{TH} shifts, the average V_{TH} shift value of GaSb NWFETs deposited with Al, Ti, Sn, Ni, and Pt is –5.2, –4.2, –7.2, 1.8, and 7.0 V, respectively. All the devices remain ohmic contact after the deposition of metals, as approved by the output characteristics of Figure S3a–c, Supporting Information. At the same time, *SS* of GaSb NWFETs is also manipulated well in expect, as shown in Figure 2e and Figure S3d–f, Supporting Information. The average *SS* decrease values of GaSb NWFETs deposited with Al, Ti, Sn, Ni, and Pt are –0.18, –0.15, –0.19, 1.18, and 7.50 V dec^{-1}, respectively. It is obvious that the *SS* and hysteresis of devices reduce after metal deposition. In general, minor *SS* and hysteresis indicate a smaller density of trap states of transistors.[56,57] The deposited low work function metal particles reduce free carriers and avoid the scattering effects, which in turn decreases the density of trap states.[5] In short, as low work function metal is deposited, *SS* of GaSb NWFETs decreases, while deposited with high work function metal, *SS* increases obviously.

Beyond the effective control of V_{TH} and *SS*, the hole mobility of GaSb NWFETs is also manipulated well by metal-semiconductor junctions, as shown in Figure 2f and Figure S3g–i, Supporting Information. Similar to the case of Al deposition, the peak hole mobility of GaSb NWFETs increases to 1938 and

© 2021 Wiley-VCH GmbH

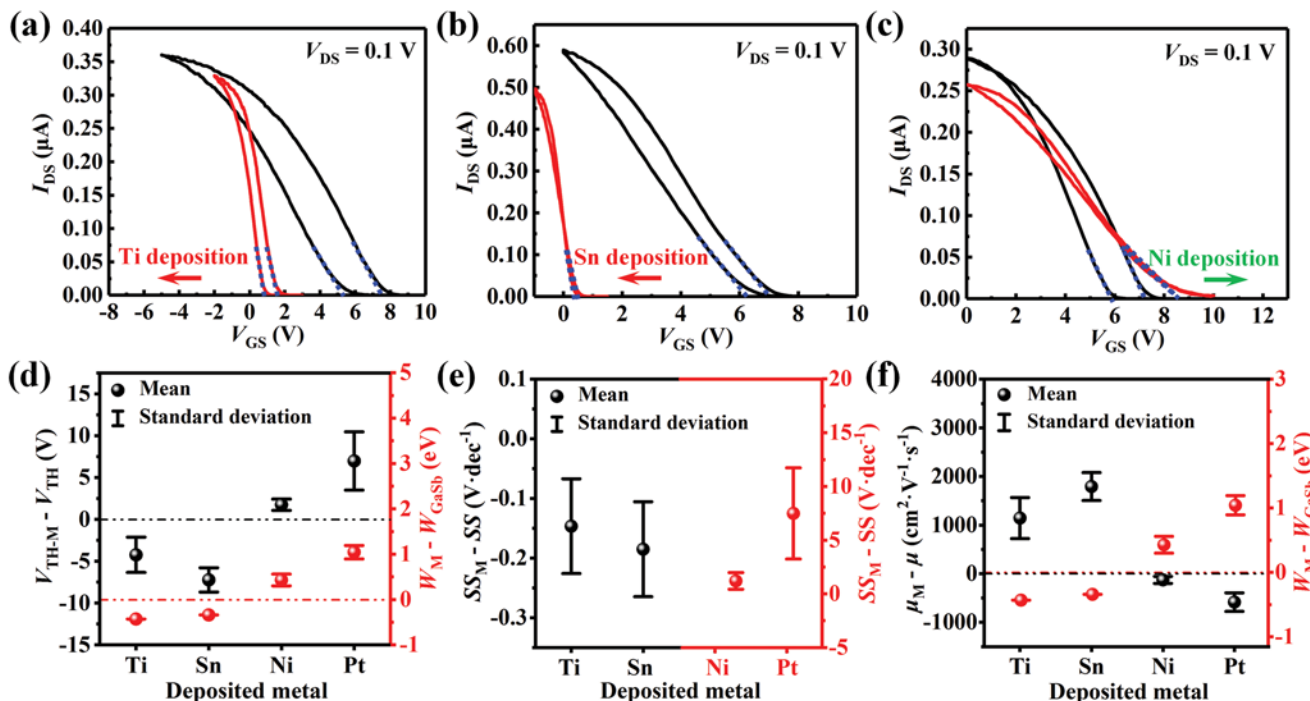

Figure 2. Generality of unusual-high hole mobility of GaSb NWFETs by metal-semiconductor junctions. a–c) Transfer characteristics of GaSb NWFETs before and after the deposition of 0.5 nm Ti, Sn and Ni film, respectively; d–f) Statistics of V_{TH} shift, *SS* decrease, and mobility enhancement of GaSb NWFETs as a function of deposition metal.

2840 cm^2 V$^{-1}\cdot$s^{-1} respectively, when the low work function metals of Ti and Sn deposited on, showing three times value than the original NWFETs. In contrast, the peak hole mobility of GaSb NWFETs reduces to 434 and 489 cm^2 V^{-1} s^{-1} respectively after the deposition of high work function metals of Ni and Pt. The averages of mobility enhancement after the deposition of Al, Ti, Sn films are 1607, 1144, and 1793 cm^2 V^{-1} s^{-1}, respectively, while, the averages of mobility decrease after the deposition of Ni and Pt are 128 and 584 cm^2 V^{-1} s^{-1}, respectively. The regulation of mobility, V_{TH}, *SS*, and hole concentration by metal-semiconductor junctions are summarized in **Table 1**. When the work function of deposited metal lower than GaSb, V_{TH} of GaSb NWFETs shifts negatively, the hole concentration decreases and the hole mobility increases. On the contrary, V_{TH} of the GaSb NWFETs shifts positively, the hole concentration increase and the hole mobility decrease when the work function of deposited metal higher than GaSb. Furthermore, with the deposition thickness increases, the shift negatively/positively of

Table 1. Mobility, V_{TH}, *SS* and hole concentration regulation of GaSb NWFETs by metal-semiconductor junctions.

Metal	Work function [eV]	Melting point [°C]	Thickness [nm]	μ_M–μ [cm^2 V^{-1} s^{-1}]	$V_{TH,M}$–V_{TH} [V]	SS_M–SS [V dec^{-1}]	$n_{h,M}$–n_h [10^{17} cm^3]
Al	4.06–4.26	660	0.1	24 ± 151	−2.1 ± 1.3	−0.09 ± 0.25	−2.5 ± 1.6
			0.5	1067 ± 503	−5.2 ± 1.2	−0.18 ± 0.07	−5.8 ± 2.5
			1	1429 ± 385	−4.8 ± 1.2	−0.11 ± 0.06	−6.0 ± 1.5
			2	1437 ± 557	−7.6 ± 1.2	−0.17 ± 0.13	−9.4 ± 1.1
Ti	4.33	1668	0.5	1144 ± 425	−4.2 ± 2.1	−0.15 ± 0.08	−4.7 ± 3.0
			1	832 ± 558	−3.6 ± 1.3	−0.04 ± 0.47	−4.5 ± 1.7
Sn	4.42	231	0.1	288 ± 164	−6.4 ± 1.2	−0.09 ± 0.06	−8.1 ± 1.6
			0.5	1793 ± 288	−7.2 ± 1.4	−0.19 ± 0.09	−9.0 ± 2.5
			1	1649 ± 422	−6.4 ± 0.7	−0.11 ± 0.06	−8.0 ± 1.5
			2	1582 ± 215	−6.7 ± 0.3	−0.08 ± 0.04	−8.4 ± 1.1
Ni	5.04–5.35	1453	0.5	−128 ± 73	1.7 ± 0.7	1.2 ± 0.8	2.2 ± 0.8
			1	−435 ± 276	7.8 ± 8.2	7.5 ± 8.9	4.6 ± 11.7
Pt	5.64–5.93	1768	0.1	−584 ± 191	7.0 ± 3.5	7.5 ± 4.1	6.3 ± 4.5
			0.5	−496 ± 337	14.9 ± 7.3	20.5 ± 17.9	18.4 ± 9.1

© 2021 Wiley-VCH GmbH

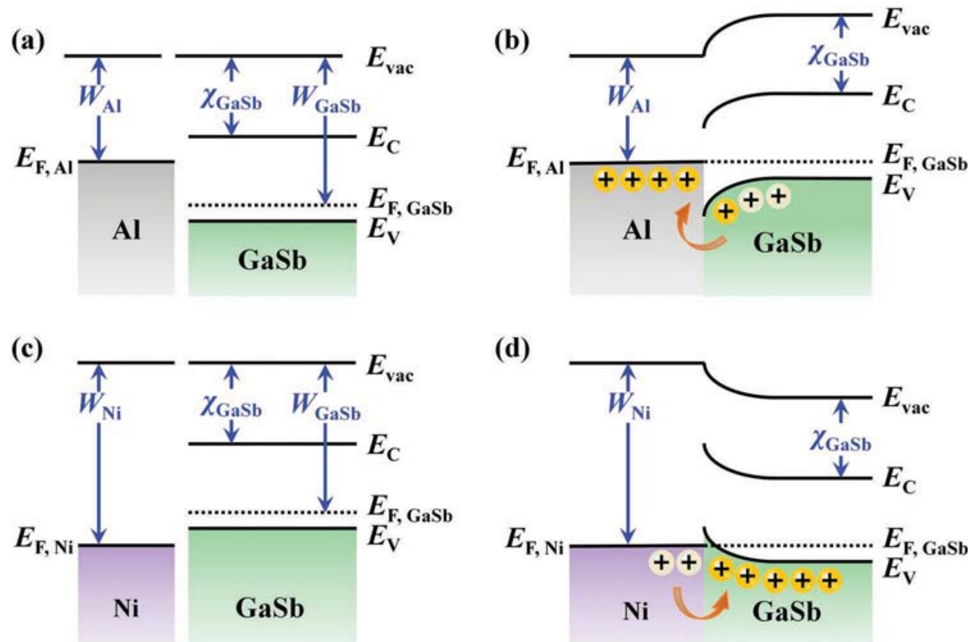

Figure 3. Schematics of unusual-high hole mobility of p-channel FETs by metal-semiconductor junctions. a,b) Energy band diagrams of low work function metal of Al and GaSb before and after constructing metal-semiconductor junctions; c,d) Energy band diagrams of high work function metal of Ni and GaSb before and after constructing metal-semiconductor junctions.

V_{TH}, the decrease/increase of hole concentration and increase/decrease of hole mobility are all in gradual. There are some values deviations observed in the case of Ti- and Sn-deposited FETs, possibly caused by the difficulty of thickness control during the deposition process. Anyway, by adopting metal-semiconductor junctions, the hole mobility of p-FETs can be enhanced efficiently.

To find out the regulation mechanism of carrier mobility, energy band diagrams of metal-semiconductor junctions are studied in detail in **Figure 3** by taking Al-GaSb junction and Ni-GaSb junction as examples. As shown in Figure 3a,c, GaSb has an energy band gap of 0.726 eV, electron affinity (χ_{GaSb}) of 4.06 eV, and work function (W_{GaSb}) of 4.76 eV, while Al has a lower work function (W_{Al}) of 4.06–4.26 eV and Ni has higher work function (W_{Ni}) of 5.04–5.35 eV. Owing to the relatively high free hole concentration, the Fermi level (E_F) of as-studied GaSb lies near the valence band edge at equilibrium. When Al film is deposited on the surface of GaSb to construct Al-GaSb junctions, as illustrated in Figure 3b, the equilibrium band diagram disturbs locally to induce a downward band-bending at Al-GaSb interface, such that the free hole flow from GaSb into Al, causing the decrease of hole concentration and the enhancement of hole mobility. On the contrary, when the metal with a higher work function, such as Ni, is deposited on the surface of GaSb to construct the Ni-GaSb junctions, the positive work function difference (W_{Ni} – W_{GaSb}) leads to an upward band-bending at Ni-GaSb interface, as shown in Figure 3d. In this case, the free hole transfer from Ni to GaSb, resulting in the increase of hole concentration and decrease of hole mobility. These kinds of band-bending and electrons transfer process always occur as soon as the semiconductors contact with metals, resulting from the work function difference (W_{metal} – W_{GaSb}). In a word, all these theoretically demonstrate the simply constructed metal-semiconductor junction here is really an efficient strategy of hole mobility enhancement.

To further demonstrate the generality of this hole mobility enhancement strategy by simply constructing metal-semiconductor junction, p-channel FETs of GaAs NW, GaAs film, and 2D WSe_2 FETs are employed in **Figure 4**. Owing to the work functions of GaAs and WSe_2 are 4.71 and 4.6–4.79 eV,[58–60] respectively, Al can be adopted as the low work function metal to construct the metal-semiconductor junctions for improving the hole mobilities. The insets of Figure 4 show the corresponding optical images of as-fabricated GaAs NW, GaAs film, and 2D WSe_2 FETs. Figure 4a shows the transfer characteristics in linear coordinates of GaAs NWFET before and after the deposition of 1 nm Al film. Obviously, after the deposition of Al film, I_{on} effectively increases from 11 to 17 pA, and V_{TH} shifts negatively. Meanwhile, the calculated $|g_m|$ of GaAs NWFET increases from 8.6 to 14.9 pS, as shown in Figure 4b, demonstrating the success in hole mobility enhancement. Besides the NW device, this hole mobility enhancement strategy is also verified in GaAs thin-film devices. Figures 4c,d illustrate the transfer characteristics and $|g_m|$ of the GaAs thin-film FET before and after the deposition of 1 nm Al film. Similarly, after constructing Al-GaAs junctions, I_{on} increases from 2.9 to 4.9 nA, and $|g_m|$ increases from 0.6 to 1.4 nS, which demonstrates more than twice the increase of hole mobility. In fact, p-type GaSb wafers are also adopted to construct the metal-semiconductor junctions for demonstrating the generality of the hole mobility enhancement strategy. As shown in Figure S5, Supporting Information, compared with that of original GaSb wafer, Hall mobility (μ_{Hall}) of the Sn-deposited GaSb wafer increases, on the other hand, μ_{Hall} of Ni-deposited GaSb wafer decreases. The variation

 © 2021 Wiley-VCH GmbH

NANO · MICRO small
www.small-journal.com

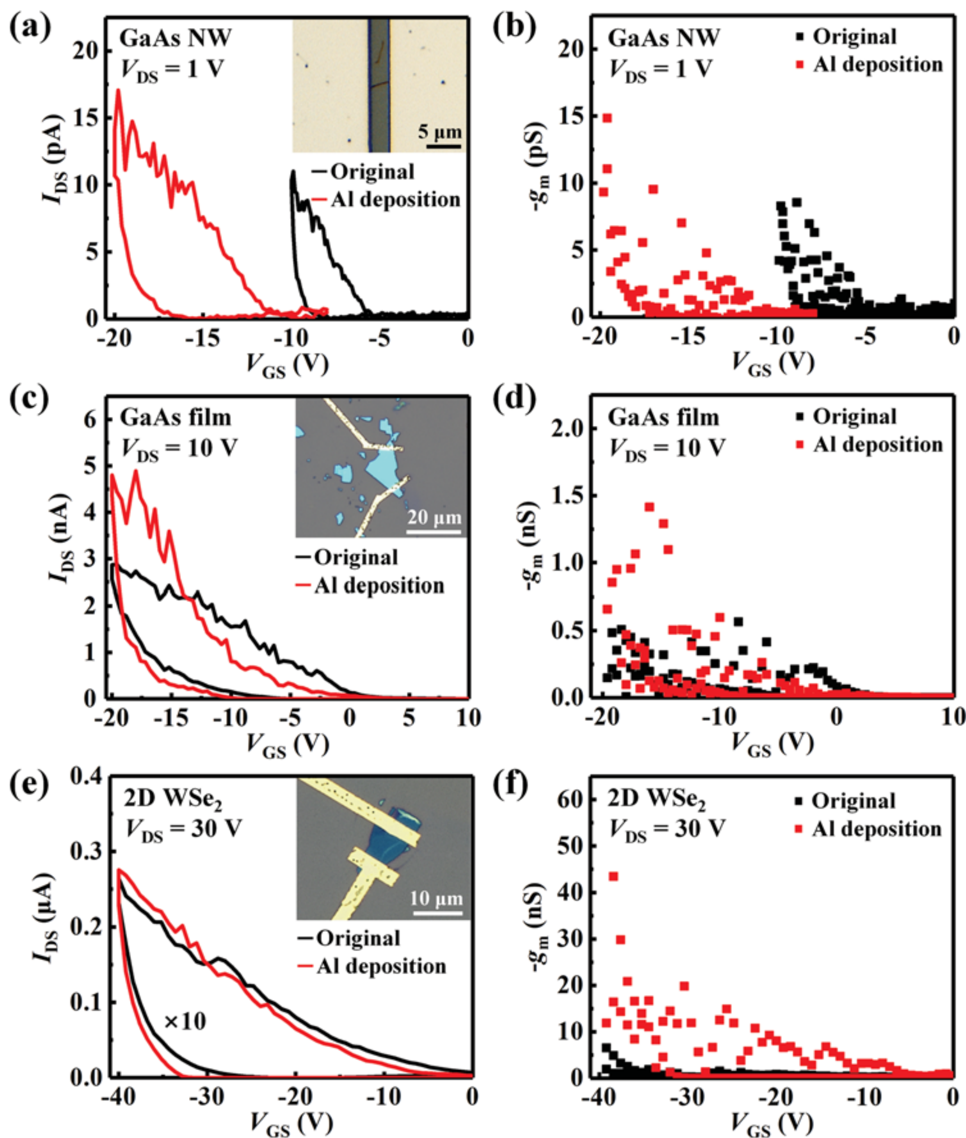

Figure 4. Generality of unusual-high hole mobility of p-channel FETs by metal-semiconductor junctions. Transfer characteristics and transconductances of a,b) GaAs NW, c,d) GaAs film, and e,f) 2D WSe_2 FETs before and after the deposition of 1 nm Al films. Insets show the corresponding optical images of as-fabricated FETs.

trends of hole concentration and μ_{Hall} are in agreement with the metal-semiconductor junctions mechanism discussed above. However, compared to NW and thin-film FETs, the hole mobility regulation of metal-deposited GaSb wafer is weak, probably attributing to the thick thickness of GaSb wafers. In this case, 2D WSe_2 with atomic scale thickness is studied in Figures 4e,f. After the deposition of 1 nm Al film, I_{on} of 2D WSe_2 FET increases from 0.03 to 0.28 μA, and $|g_m|$ increases from 6.5 to 43.5 nS, proving a six to seven times increase of hole mobility. Obviously, this metal-semiconductor junction is more efficient for atomic scale 2D semiconductors than NWs, thin film, and wafer, which is mainly because the thickness of 2D material is the thinnest and the carriers are easiest to be controlled. However, the hysteresis is still large even with the metal coverage, some strategies can be employed to eliminate or reduce the acceptable levels. Interface engineering provides an effective and promising approach to reduce hysteresis in transistor. By treating the semiconductor/dielectric interfaces with plasma ozone and self-assembled monolayer (Octadecyltrichlorosilane, octadecylphosphonic acids, hexamethyldisilazane, and the like) can effectively improve the smoothness and surface energies, thus reducing the hysteresis.[61] In brief, all the results demonstrate the simply constructed metal-semiconductor junction here is an efficient strategy for hole mobility enhancement.

After achieving unusual-high hole mobility, negative shifted V_{TH}, decreased SS, and remained I_{on}/I_{off}, Al-GaSb NWFET is constructed with n-type InGaAs NWFET to demonstrate the potential application in CMOS inverter. **Figure 5a** shows the transfer characteristics of the driver (GaSb NWFET deposited with 0.5 nm Al film) and the load (InGaAs NWFET) at V_{DS} = 0.1 V. V_{TH} of Al-GaSb NWFET is between 1.2 and

 © 2021 Wiley-VCH GmbH

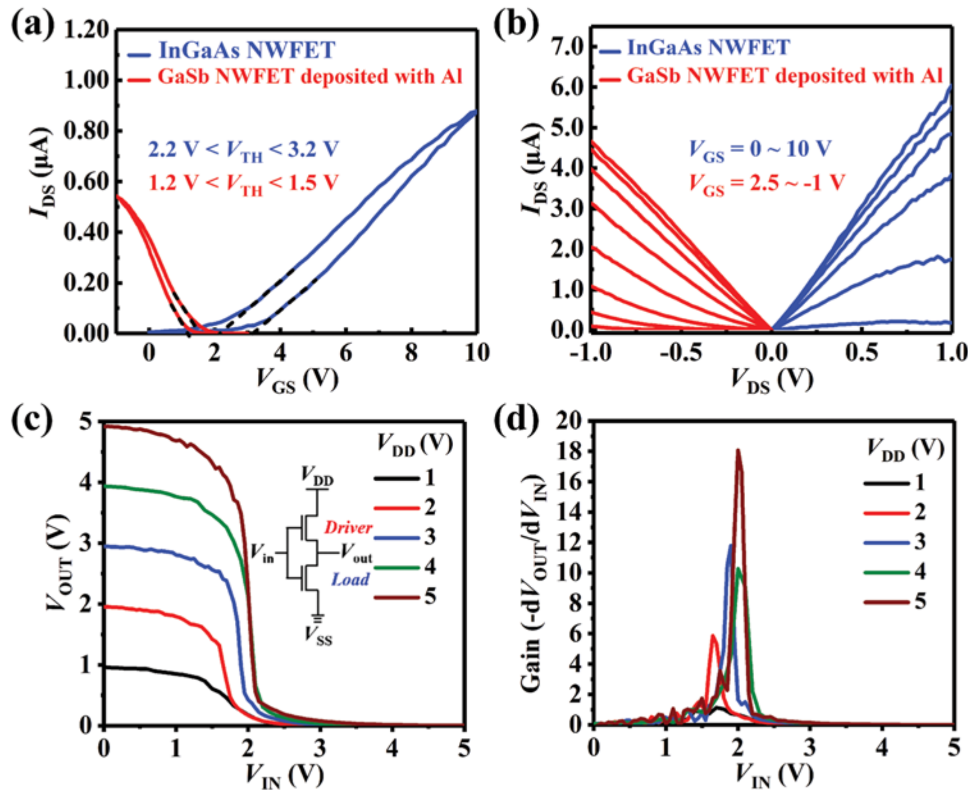

Figure 5. CMOS inverter constructed by the obtained unusual-high hole mobility GaSb NWFETs. a,b) Transfer and output characteristics of the driver (GaSb NWFET deposited with 0.5 nm Al film) and the load (InGaAs NWFET); c) the voltage transfer characteristics (VTC) of the as-fabricated CMOS inverter at different V_{DD}. The inset shows the schematic circuit diagram of the inverter; d) the voltage gain extracted by differentiating VTC.

1.5 V, and V_{TH} of InGaAs NWFET is between 2.2 and 3.2 V. V_{TH} separation between n- and p-type FETs is important in CMOS invert, ensuring the driver and load do not open at the same time. In this case, there is no direct path exists between the supply and ground rails under steady-state operating conditions, resulting in the lower power dissipation.[62] The output characteristics of driver and load are shown in Figure 5b, indicating the ohmic contact and symmetric performance of both n- and p-type FETs. The uniform and symmetric performance of p- and n-type FETs will benefit to the obtain of high-performance CMOS invert.[62] As shown in the voltage transfer characteristics (VTC) of the CMOS inverter of Figure 5c, it is obvious that the inverter can efficiently alter the logic “0” (low V_{IN}) into the logic “1” (high V_{OUT}) and vice versa under V_{DD} of 1–5 V when V_{IN} swings from 0 to 5 V. The schematic circuit diagram of the inverter is shown in the inset of Figure 5c. It is also worth noting that the inverter can function at a relatively low voltage of ≈2.5 V, along with the insignificant leakage current and reduced power consumption. In the end, benefiting from the matched mobility and separated V_{TH} between n- and p-FETs, the input signal is inverted with a relatively high gain of ≈18.1 for V_{DD} = 5 V and the CMOS inverter exhibits good time-resolved property at 100 Hz frequency under V_{DD} = 8 V (Figure 5d and Figure S6, Supporting Information), which is comparable to previous reports.[63] Further performance enhancements of CMOS invert can be achieved by optimizing device geometry for reducing the parasitic capacitance and so on.

3. Conclusion

In conclusion, metal-semiconductor junction constructed by depositing CMOS-compatible metals with lower work function has been demonstrated as an efficient strategy of hole mobility enhancement for p-channel building block device, owing to the downward band-bending at the metal-semiconductor interface and the reduced hole concentration by the injection of electrons from deposited metals. The peak hole mobility of as-studied GaSb NWFET can be enhanced as high as 3372 cm^2 V^{-1} s^{-1} after constructing Al-GaSb junctions, showing three times value than the original NWFET, which is the highest values among p-channel FETs in the atmosphere. This hole mobility enhancement strategy is generalized and can also modify the hole mobility of other p-channel devices, such as GaAs NWFET, GaAs film FET, and 2D WSe_2 FET. Constructed by the unusual-high hole mobility Al-GaSb NWFET, the as-fabricated CMOS inverter exhibits good invert characteristics with a relatively high gain of ≈18.1. The reported metal-semiconductor junctions here can be regarded as important advances in the high hole mobility p-channel building block devices and promotes the development of next-generation electronics.

Supporting Information

Supporting Information is available from the Wiley Online Library or from the author.

© 2021 Wiley-VCH GmbH

Acknowledgements

J.M.S. and X.M.Z. contributed equally to this work. The authors acknowledge the National Key R&D Program of China (No. 2017YFA0305500), National Natural Science Foundation of China (No. 61904096), Taishan Scholars Program of Shandong Province (No. tsqn201812006), Shandong University multidisciplinary research and innovation team of young scholars (No. 2020QNQT015), "Outstanding youth scholar and Qilu young scholar" programs of Shandong University, and the Youth Interdisciplinary Science and Innovative Research Groups of Shandong University.

Conflict of Interest

The authors declare no conflict of interest.

Data Availability Statement

The data that support the findings of this study are available from the corresponding author upon reasonable request.

Keywords

carrier concentration control, field-effect-transistors, GaSb nanowires, hole mobility, metal-semiconductor junction

Received: April 20, 2021
Revised: June 27, 2021
Published online:

[1] J. A. del Alamo, *Nature* **2011**, *479*, 317.
[2] K. Myny, *Nat. Electron.* **2018**, *1*, 30.
[3] X. Yuan, D. Pan, Y. Zhou, X. Zhang, K. Peng, B. Zhao, M. Deng, J. He, H. H. Tan, C. Jagadish, *Appl. Phys. Rev.* **2021**, *8*, 021302.
[4] D.-H. Park, Y. J. Cho, J.-H. Lee, I. Choi, S. H. Jhang, H.-J. Chung, *Nanotechnology* **2019**, *30*, 394003.
[5] F. Li, S. Yip, R. Dong, Z. Zhou, C. Lan, X. Liang, D. Li, Y. Meng, X. Kang, J. C. Ho, *Nano Res.* **2019**, *12*, 1796.
[6] Z. Wu, Z. Jiang, P. Song, P. Tian, L. Hu, R. Liu, Z. Fang, J. Kong, T.-Y. Zhang, *Small* **2019**, *15*, 1900580.
[7] Y. Xu, X. Shi, Y. Zhang, H. Zhang, Q. Zhang, Z. Huang, X. Xu, J. Guo, H. Zhang, L. Sun, Z. Zeng, A. Pan, K. Zhang, *Nat. Commun.* **2020**, *11*, 1330.
[8] J. Sun, Y. Yin, M. Han, Z.-x. Yang, C. Lan, L. Liu, Y. Wang, N. Han, L. Shen, X. Wu, J. C. Ho, *ACS Nano* **2018**, *12*, 10410.
[9] Y. Zhao, J. Qiao, Z. Yu, P. Yu, K. Xu, S. P. Lau, W. Zhou, Z. Liu, X. Wang, W. Ji, Y. Chai, *Adv. Mater.* **2017**, *29*, 1604230.
[10] W. Feng, W. Zheng, W. Cao, P. Hu, *Adv. Mater.* **2014**, *26*, 6587.
[11] A. N. Rudenko, S. Brener, M. I. Katsnelson, *Phys. Rev. Lett.* **2016**, *116*, 246401.
[12] J. Wu, C. Qiu, H. Fu, S. Chen, C. Zhang, Z. Dou, C. Tan, T. Tu, T. Li, Y. Zhang, Z. Zhang, L.-M. Peng, P. Gao, B. Yan, H. Peng, *Nano Lett.* **2019**, *19*, 197.
[13] R. Dingle, H. L. Stormer, A. C. Gossard, W. Wiegmann, *Appl. Phys. Lett.* **1978**, *33*, 665.
[14] W. Shi, S. Kahn, L. Jiang, S.-Y. Wang, H.-Z. Tsai, D. Wong, T. Taniguchi, K. Watanabe, F. Wang, M. F. Crommie, A. Zettl, *Nat. Electron.* **2020**, *3*, 99.
[15] S. M. Sze, K. K. Ng, *Physics of semiconductor devices*, John Wiley & Sons, Hoboken, NJ **2006**.
[16] J. Sun, M. Peng, Y. Zhang, L. Zhang, R. Peng, C. Miao, D. Liu, M. Han, R. Feng, Y. Ma, *Nano Lett.* **2019**, *19*, 5920.
[17] F. Wang, S. Yip, G. Dong, F. Xiu, L. Song, Z. Yang, D. Li, T. F. Hung, N. Han, J. C. Ho, *Adv. Mater. Interfaces* **2017**, *4*, 1700260.
[18] N. Han, F. Wang, J. J. Hou, S. P. Yip, H. Lin, F. Xiu, M. Fang, Z.-x. Yang, X. Shi, G. Dong, T. F. Hung, J. C. Ho, *Adv. Mater.* **2013**, *25*, 4445.
[19] S. Mubeen, M. Moskovits, *Adv. Mater.* **2011**, *23*, 2306.
[20] Y. Hirose, A. Kahn, V. Aristov, P. Soukiassian, V. Bulovic, S. R. Forrest, *Phys. Rev. B* **1996**, *54*, 13748.
[21] Z.-x. Yang, S. Yip, D. Li, N. Han, G. Dong, X. Liang, L. Shu, T. F. Hung, X. Mo, J. C. Ho, *ACS Nano* **2015**, *9*, 9268.
[22] Z.-x. Yang, L. Liu, S. Yip, D. Li, L. Shen, Z. Zhou, N. Han, T. F. Hung, E. Y. Pun, X. Wu, A. Song, J. C. Ho, *ACS Nano* **2017**, *11*, 4237.
[23] A. Liu, G. Liu, H. Zhu, H. Song, B. Shin, E. Fortunato, R. Martins, F. Shan, *Adv. Funct. Mater.* **2015**, *25*, 7180.
[24] H. Zhu, A. Liu, G. Liu, F. Shan, *Appl. Phys. Lett.* **2017**, *111*, 143501.
[25] J. A. Caraveo-Frescas, H. N. Alshareef, *Appl. Phys. Lett.* **2013**, *103*, 222103.
[26] K. J. Saji, K. Tian, M. Snure, A. Tiwari, *Adv. Electron. Mater.* **2016**, *2*, 1500453.
[27] C. W. Shih, A. Chin, C. F. Lu, W. F. Su, *Sci. Rep.* **2018**, *8*, 889.
[28] X. Guan, Z. Wang, M. K. Hota, H. N. Alshareef, T. Wu, *Adv. Electron. Mater.* **2019**, *5*, 1800538.
[29] Q. Cao, Y.-W. Dai, J. Xu, L. Chen, H. Zhu, Q.-Q. Sun, D. W. Zhang, *ACS Appl. Mater. Interfaces* **2017**, *9*, 18215.
[30] B. Tang, Z. G. Yu, L. Huang, J. Chai, S. L. Wong, J. Deng, W. Yang, H. Gong, S. Wang, K.-W. Ang, Y.-W. Zhang, D. Chi, *ACS Nano* **2018**, *12*, 2506.
[31] H. Chen, Y. Cao, J. Zhang, C. Zhou, *Nat. Commun.* **2014**, *5*, 4097.
[32] B. Chen, P. Zhang, L. Ding, J. Han, S. Qiu, Q. Li, Z. Zhang, L.-M. Peng, *Nano Lett.* **2016**, *16*, 5120.
[33] J. M. Salazar-Rios, A. A. Sengrian, W. Talsma, H. Duim, M. Abdu-Aguye, S. Jung, N. Froehlich, S. Allard, U. Scherf, M. A. Loi, *Adv. Electron. Mater.* **2020**, *6*, 1900789.
[34] F. Shan, A. Liu, H. Zhu, W. Kong, J. Liu, B. Shin, E. Fortunato, R. Martins, G. Liu, *J. Mater. Chem. C* **2016**, *4*, 9438.
[35] C. Zhao, C. Tan, D.-H. Lien, X. Song, M. Amani, M. Hettick, H. Y. Y. Nyein, Z. Yuan, L. Li, M. C. Scott, A. Javey, *Nat. Nanotechnol.* **2020**, *15*, 53.
[36] A. Pezeshki, S. H. H. Shokouh, P. J. Jeon, I. Shackery, J. S. Kim, I.-K. Oh, S. C. Jun, H. Kim, S. Im, *ACS Nano* **2016**, *10*, 1118.
[37] D. Qu, X. Liu, M. Huang, C. Lee, F. Ahmed, H. Kim, R. S. Ruoff, J. Hone, W. J. Yoo, *Adv. Mater.* **2017**, *29*, 1606433.
[38] E. Wu, Y. Xie, J. Zhang, H. Zhang, X. Hu, J. Liu, C. Zhou, D. Zhang, *Sci. Adv.* **2019**, *5*, eaav3430.
[39] X. Liu, D. Qu, J. Ryu, F. Ahmed, Z. Yang, D. Lee, W. J. Yoo, *Adv. Mater.* **2016**, *28*, 2345.
[40] S.-W. Min, M. Yoon, S. J. Yang, K. R. Ko, S. Im, *ACS Appl. Mater. Interfaces* **2018**, *10*, 4206.
[41] J. Guo, Y. Liu, Y. Ma, E. Zhu, S. Lee, Z. Lu, Z. Zhao, C. Xu, S.-J. Lee, H. Wu, K. Kovnir, Y. Huang, X. Duan, *Adv. Mater.* **2018**, *30*, 1705934.
[42] P. M. Campbell, A. Tarasov, C. A. Joiner, M.-Y. Tsai, G. Pavlidis, S. Graham, W. J. Ready, E. M. Vogel, *Nanoscale* **2016**, *8*, 2268.
[43] P. R. Pudasaini, A. Oyedele, C. Zhang, M. G. Stanford, N. Cross, A. T. Wong, A. N. Hoffman, K. Xiao, G. Duscher, D. G. Mandrus, T. Z. Ward, P. D. Rack, *Nano Res.* **2018**, *11*, 722.
[44] R. Tu, L. Zhang, Y. Nishi, H. Dai, *Nano Lett.* **2007**, *7*, 1561.
[45] M. Simanullang, G. B. M. Wisna, K. Usami, W. Cao, Y. Kawano, K. Banerjee, S. Oda, *J. Mater. Chem. C* **2016**, *4*, 5102.
[46] Y. Li, R. Zhang, *Appl. Phys. Lett.* **2019**, *114*, 132101.
[47] Z.-x. Yang, N. Han, F. Wang, H.-Y. Cheung, X. Shi, S. Yip, T. Hung, M. H. Lee, C.-Y. Wong, J. C. Ho, *Nanoscale* **2013**, *5*, 9671.
[48] L. Li, Y. Yu, G. J. Ye, Q. Ge, X. Ou, H. Wu, D. Feng, X. H. Chen, Y. Zhang, *Nat. Nanotechnol.* **2014**, *9*, 372.

 © 2021 Wiley-VCH GmbH

[49] W. C. Tan, Y. Cai, R. J. Ng, L. Huang, X. Feng, G. Zhang, Y.-W. Zhang, C. A. Nijhuis, X. Liu, K.-W. Ang, *Adv. Mater.* **2017**, *29*, 1700503.
[50] X. Feng, X. Huang, L. Chen, W. C. Tan, L. Wang, K.-W. Ang, *Adv. Funct. Mater.* **2018**, *28*, 1801524.
[51] D. He, Y. Wang, Y. Huang, Y. Shi, X. Wang, X. Duan, *Nano Lett.* **2019**, *19*, 331.
[52] Z.-x. Yang, F. Wang, N. Han, H. Lin, H. Y. Cheung, M. Fang, S. Yip, T. Hung, C. Y. Wong, J. C. Ho, *ACS Appl. Mater. Interfaces* **2013**, *5*, 10946.
[53] Z.-x. Yang, N. Han, M. Fang, H. Lin, H. Y. Cheung, S. Yip, E. J. Wang, T. Hung, C. Y. Wong, J. C. Ho, *Nat. Commun.* **2014**, *5*, 5249.
[54] M. Yokoyama, H. Yokoyama, M. Takenaka, S. Takagi, *Appl. Phys. Lett.* **2015**, *106*, 073503.
[55] G. Long, D. Maryenko, J. Shen, S. Xu, J. Hou, Z. Wu, W. K. Wong, T. Han, J. Lin, Y. Cai, R. Lortz, N. Wang, *Nano Lett.* **2016**, *16*, 7768.
[56] C. Lan, S. Yip, X. Kang, Y. Meng, X. Bu, J. C. Ho, *ACS Appl. Mater. Interfaces* **2020**, *12*, 56330.
[57] X. Zhuang, W. Huang, S. Han, Y. Jiang, H. Zheng, J. Yu, *Org. Electron.* **2017**, *49*, 334.
[58] G. W. Gobeli, F. G. Allen, *Phys. Rev.* **1965**, *137*, A245.
[59] S. Seo, S. Kim, H. Choi, J. Lee, H. Yoon, G. Piao, J.-C. Park, Y. Jung, J. Song, S. Y. Jeong, H. Park, S. Lee, *Adv. Sci.* **2019**, *6*, 1900301.
[60] T. Guo, C. Ling, T. Zhang, H. Li, X. Li, X. Chang, L. Zhu, L. Zhao, Q. Xue, *J. Mater. Chem. C* **2018**, *6*, 5821.
[61] H. Chen, W. Zhang, M. Li, G. He, X. Guo, *Chem. Rev.* **2020**, *120*, 2879.
[62] Z. Zhang, S. Wang, Z. Wang, L. Ding, T. Pei, Z. Hu, X. Liang, Q. Chen, Y. Li, L.-M. Peng, *ACS Nano* **2009**, *3*, 3781.
[63] A. W. Dey, J. Svensson, B. M. Borg, M. Ek, L.-E. Wernersson, *Nano Lett.* **2012**, *12*, 5593.

© 2021 Wiley-VCH GmbH

In the past decades, the control on carrier concentration of channel semiconductors has been considered as an efficient way to regulate the carrier mobility of building block devices.[11–12] Doping is the most memorable and useful method to realize the control of carrier concentration.[13–14] Generally speaking, the carrier mobility of intrinsic semiconductors increases with the decrease of carrier concentration.[15] In this case, it should be noticed that the concentration and kinds of the dopant are important, otherwise, the additionally introduced carrier and crystal defects will increase the carrier concentration and transport scattering, resulting in the decrease of carrier mobility.[16] As a result, it is rare to report the carrier concentration decrease and mobility increase of channel semiconductors by doping in the literature. For intrinsic p-type semiconductors, slight doping will help to improve the crystallinity quality and decrease the hole concentration, resulting in the enhanced hole mobility.[16] Beyond doping, the carrier concentration of channel semiconductors also can be controlled by constructing metal-semiconductor junctions in the building block devices.[17–18] When the semiconductors contact with the lower work function metals, the electrons from metal will inject into semiconductors, resulting in the increase of electron concentration in n-type semiconductors or the decrease of hole concentration in p-type semiconductors. On the other hand, the electron concentration will decrease in n-type semiconductors or hole concentration will increase in p-type semiconductors when the semiconductors contact with the higher work function metals. In a word, the electron mobility of the n-channel building block device will increase by contacting with the higher work function metals, otherwise, the hole mobility of the p-channel building block device will increase by contacting with the lower work function metals.[15]

Metal-semiconductor junctions can be realized easily by depositing metal nanoparticles on the surface of the building block device.[19] Although several works have focused on the threshold voltage (V_{TH}) manipulation of the n-channel building block device by metal-semiconductor junctions,[17–18] it is still a lacking of detailed investigation of hole mobility manipulation on p-channel building block device. Furthermore, in the modern electronic chips, complementary metal-oxide semiconductor (CMOS)-compatible metals of Al, Sn, Ti, etc. always have low work functions,[20] benefiting the achievement of high hole mobility p-channel building blocks device. In this work, GaSb NW has been selected as the studied p-channel semiconductor, owing to its highest hole mobility among all III–V group semiconductors and the development of high-performance all-around-gated one-dimensional NWFETs has been considered as an optimal solution for the continuation of Moore's Law in the near future.[16,21,22] When deposited with the low work function metals of Al, Sn, and Ti, the peak hole mobilities of GaSb NWFETs are as high as 3372, 1938, and 2840 cm^2 V^{-1} s^{-1}, respectively. At the same time, the other important electronic properties of GaSb NWFETs, such as V_{TH}, and subthreshold (SS) also manipulated well in expect. Importantly, when connected with n-type InGaAs NWs, the fabricated CMOS invert shows good invert characteristics with a relatively high gain of ≈18.1, benefiting from the enhanced hole mobility, the manipulated V_{TH}, and SS, etc. This hole mobility enhancement strategy is also efficient in other p-channel devices, such as GaAs NWFET, GaAs film FET, and 2D WSe_2 FET. All results confirm the promise of these unusual-high hole mobility FETs obtained by metal-semiconductor junction for a wide range of applications in future technology.

2. Results and Discussion

For achieving unusual-high hole mobility, CMOS-compatible metals with different low work functions are adopted here for constructing metal-semiconductor junctions to demonstrate the hole mobility regulation of p-channel GaSb NWFETs. As shown in **Figure 1**, unusual-high hole mobility of GaSb NWFETs are achieved by constructing Al-GaSb junctions. Figure 1a illustrates the typical atomic force microscopy image of GaSb NWFET after the deposition of 0.5 nm Al film, displaying the uniform dispersion of metal nanoparticles on the surface of NWFET. The NW length in the channel is around 3 µm and the diameter is around 30 nm. Figure 1b shows the transfer characteristics in linear coordinates of the GaSb NWFET before and after the deposition of 0.5 nm Al film. Obviously, the deposition of Al film can effectively shift V_{TH} negatively, from 6.8 to 1.5 V. The lower V_{TH} illustrates the easier regulation of FETs under low gate voltage. At the same time, FETs remain ohmic contact after the construction of Al-GaSb junctions, which can be proved by the output characteristics of Figure S1a, Supporting Information. To study the thickness effect of deposition metal film, other thicknesses of 0.1, 1, and 2 nm Al films are also deposited on the surfaces of GaSb NWFETs, respectively. As shown in the transfer characteristics of Figure S1b–d, Supporting Information and the statistics of the V_{TH} shift of Figure 1c, it is obvious that the shift value of V_{TH} increases with the thickness increase of Al film. The mean value of V_{TH} shift is -2.1, −5.2, −4.8, and −7.6 V, respectively, by depositing 0.1, 0.5, 1, and 2 nm Al film. Besides the observation of V_{TH} shift, SS showed in Figure S2a, Supporting Information also decrease from 0.32 to 0.13 V dec^{-1} but I_{on}/I_{off} remains of 10^4 orders. Obviously, all these results will benefit the mobility enhancement of GaSb NWFETs.

With the negative shifted V_{TH}, decreased SS, and remained I_{on}/I_{off}, FE hole mobility of GaSb NWFETs increases significantly, as shown in Figure 1d. The peak hole mobility of GaSb NWFET increases from 1214 to 3372 cm^2 V^{-1} s^{-1} after the construction of Al-GaSb junctions. The hole mobility is calculated by using the analytical equation of $\mu = g_m \times (L^2/C_{OX}) \times (1/V_{DS})$, where the transconductance (g_m) can be extracted from the transfer characteristics following the equation of $g_m = (dI_{DS})/(dV_{GS})|V_{DS}$, and C_{OX} is the gate capacitance obtained from the finite element analysis software COMSOL with respect to different NW diameters. With different thicknesses of Al films, the mean value of mobility increase is 24.1, 1607, 1429, and 1437cm^2 V^{-1} s^{-1} respectively, as shown in Figure 1e. The mobility enhancement is unobvious after the deposition of 0.1 nm Al film, which is probably because of the low density of Al nanoparticles on the surface of GaSb NWs. On the other hand, the hole mobility of the FETs deposited with 2 nm Al film shows a little lower value than ones deposited with 0.5 nm Al film. The sizes of Al nanoparticles would be larger in 2 nm Al film than 0.5 nm film, leading to the less efficient carrier injunction channel between

 © 2021 Wiley-VCH GmbH

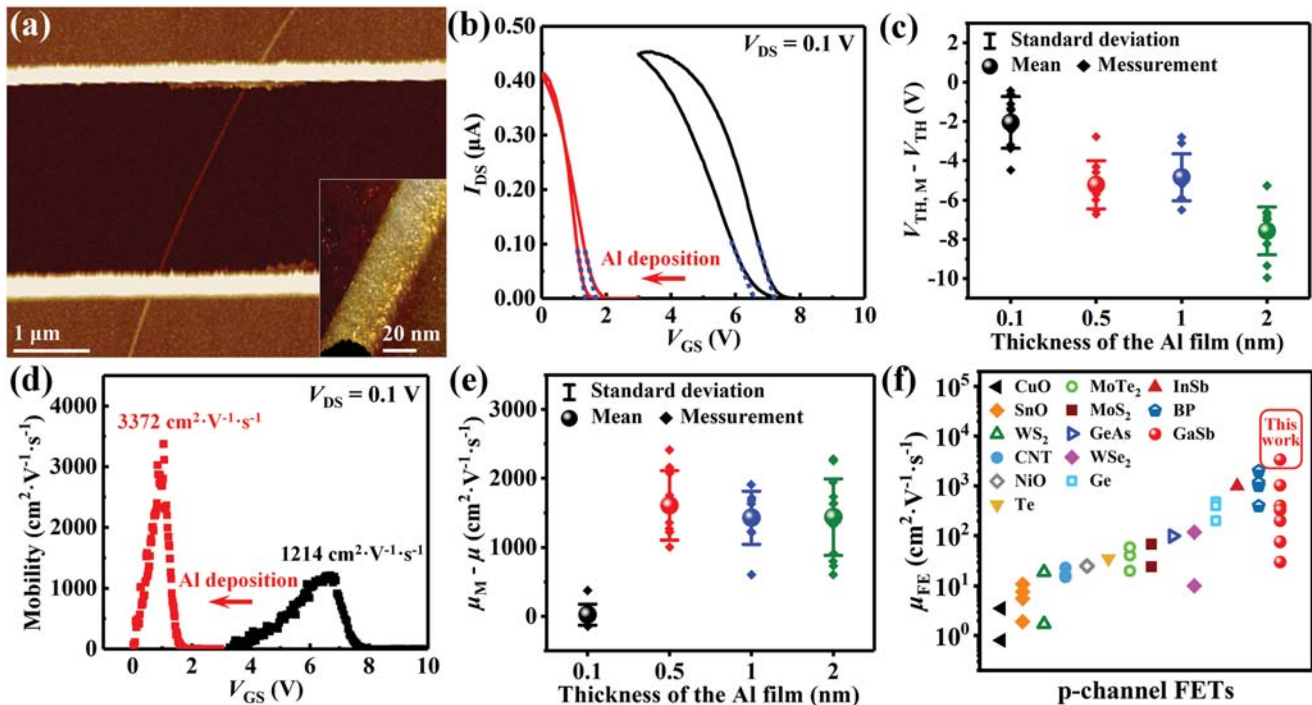

Figure 1. Toward unusual-high hole mobility of GaSb NWFETs by Al-GaSb junctions. a) Typical atomic force microscopy (AFM) image of GaSb NWFET deposited with 0.5 nm Al film. Inset shows the corresponding three-dimensional AFM image of channel GaSb NW; b) transfer characteristics of GaSb NWFET before and after the deposition of Al film; c) V_{TH} shift statistics of GaSb NWFETs deposited with different thicknesses of Al films (V_{DS} = 0.1 V); d) field-effect (FE) mobility of GaSb NWFET before and after depositing 0.5 nm Al film; e) statistics of mobility enhancement of GaSb NWFETs as function of Al film thickness (V_{DS} = 0.1 V); f) FE hole mobilities of typical p-channel (CuO,[23,24] SnO,[25–28] WS_2,[29,30] CNT,[31–33] NiO,[34] Te,[35] $MoTe_2$,[36–38] MoS_2,[39,40] GeAs,[41] WSe_2,[42,43] Ge,[44–46] InSb,[47] BP,[48–51] GaSb[16,21–22,52–54]) FETs in the literatures (at room temperature in the atmosphere).

Al and GaSb. Anyway, this phenomenon is interesting and will be studied in the near future. Especially, the demonstrated unusual-high hole mobility of 3372 $cm^2 V^{-1} s^{-1}$ in this work is the highest room-temperature value among p-channel FETs in the atmosphere in the literature. As shown in Figure 1f, most of the p-channel FETs, such as p-type oxide semiconductor TFTs of CuO,[23,24] SnO,[25–28] NiO,[34] and typical p-type 2D transition-metal dichalcogenides FETs of WS_2,[29,30] $MoTe_2$,[36–38] MoS_2,[39,40] WSe_2,[42,43] exhibit the hole mobilities between the order of 10^0 to 10^2 $cm^2 V^{-1} s^{-1}$. Recently, few-layer black phosphorus (BP)-based FET is also considered as one of the good candidates for p-channel building blocks, as its reported FE hole mobility can reach up to 5200 $cm^2 V^{-1} s^{-1}$.[55] However, the device fabrication and measurement processes require a vacuum environment rather than in the atmosphere, challenging further applications in electronics and optoelectronics. In short, the deposition of low work function metal of Al on the surface of GaSb NWFETs is really an efficient hole mobility enhancement strategy.

To shed light on the mobility regulation mechanism, metal films with different work functions are deposited on GaSb NWFETs to construct metal-semiconductor junctions, along with the systematic investigation of electrical properties. As shown in **Figure 2**a,b, with the deposition of lower work function metals of Ti and Sn (4.33 eV for Ti and 4.42 eV for Sn), V_{TH} of GaSb NWFET shifts negatively, from 6.4 to 1.1 V, and from 6.5 to 0.4 V, respectively. On the contrary, V_{TH} of GaSb NWFET shifts positively, from 6.5 to 8.4 V and from 5.6 to 15.3 V, respectively, when the higher work function metals of Ni (5.04–5.35 eV) and Pt (5.64–5.93 eV) are deposited, as shown in Figure 2c and Figure S4, Supporting Information, which mainly because of the hole concentration increase and require a larger gate voltage to realize the regulation of FETs. As shown in Figure 2d of the statistics of V_{TH} shifts, the average V_{TH} shift value of GaSb NWFETs deposited with Al, Ti, Sn, Ni, and Pt is –5.2, –4.2, –7.2, 1.8, and 7.0 V, respectively. All the devices remain ohmic contact after the deposition of metals, as approved by the output characteristics of Figure S3a–c, Supporting Information. At the same time, *SS* of GaSb NWFETs is also manipulated well in expect, as shown in Figure 2e and Figure S3d–f, Supporting Information. The average *SS* decrease values of GaSb NWFETs deposited with Al, Ti, Sn, Ni, and Pt are –0.18, –0.15, –0.19, 1.18, and 7.50 V dec^{-1}, respectively. It is obvious that the *SS* and hysteresis of devices reduce after metal deposition. In general, minor *SS* and hysteresis indicate a smaller density of trap states of transistors.[56,57] The deposited low work function metal particles reduce free carriers and avoid the scattering effects, which in turn decreases the density of trap states.[5] In short, as low work function metal is deposited, *SS* of GaSb NWFETs decreases, while deposited with high work function metal, *SS* increases obviously.

Beyond the effective control of V_{TH} and *SS*, the hole mobility of GaSb NWFETs is also manipulated well by metal-semiconductor junctions, as shown in Figure 2f and Figure S3g–i, Supporting Information. Similar to the case of Al deposition, the peak hole mobility of GaSb NWFETs increases to 1938 and

 © 2021 Wiley-VCH GmbH

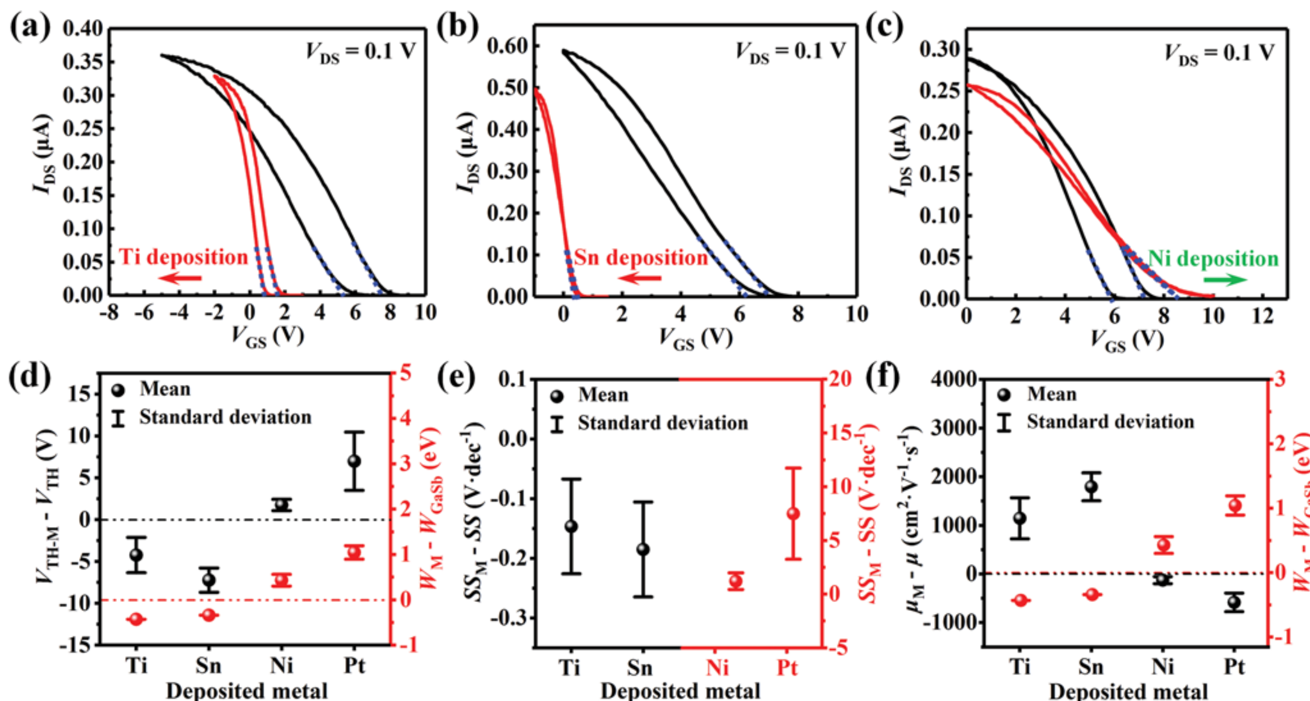

Figure 2. Generality of unusual-high hole mobility of GaSb NWFETs by metal-semiconductor junctions. a–c) Transfer characteristics of GaSb NWFETs before and after the deposition of 0.5 nm Ti, Sn and Ni film, respectively; d–f) Statistics of V_{TH} shift, *SS* decrease, and mobility enhancement of GaSb NWFETs as a function of deposition metal.

2840 cm^2 V^{-1}·s^{-1} respectively, when the low work function metals of Ti and Sn deposited on, showing three times value than the original NWFETs. In contrast, the peak hole mobility of GaSb NWFETs reduces to 434 and 489 cm^2 V^{-1} s^{-1} respectively after the deposition of high work function metals of Ni and Pt. The averages of mobility enhancement after the deposition of Al, Ti, Sn films are 1607, 1144, and 1793 cm^2 V^{-1} s^{-1}, respectively, while, the averages of mobility decrease after the deposition of Ni and Pt are 128 and 584 cm^2 V^{-1} s^{-1}, respectively. The regulation of mobility, V_{TH}, *SS*, and hole concentration by metal-semiconductor junctions are summarized in **Table 1**. When the work function of deposited metal lower than GaSb, V_{TH} of GaSb NWFETs shifts negatively, the hole concentration decreases and the hole mobility increases. On the contrary, V_{TH} of the GaSb NWFETs shifts positively, the hole concentration increase and the hole mobility decrease when the work function of deposited metal higher than GaSb. Furthermore, with the deposition thickness increases, the shift negatively/positively of

Table 1. Mobility, V_{TH}, *SS* and hole concentration regulation of GaSb NWFETs by metal-semiconductor junctions.

Metal	Work function [eV]	Melting point [°C]	Thickness [nm]	μ_M–μ [cm^2 V^{-1} s^{-1}]	$V_{TH,M}$–V_{TH} [V]	SS_M–SS [V dec^{-1}]	$n_{h,M}$–n_h [10^{17} cm^3]
Al	4.06–4.26	660	0.1	24 ± 151	−2.1 ± 1.3	−0.09 ± 0.25	−2.5 ± 1.6
			0.5	1067 ± 503	−5.2 ± 1.2	−0.18 ± 0.07	−5.8 ± 2.5
			1	1429 ± 385	−4.8 ± 1.2	−0.11 ± 0.06	−6.0 ± 1.5
			2	1437 ± 557	−7.6 ± 1.2	−0.17 ± 0.13	−9.4 ± 1.1
Ti	4.33	1668	0.5	1144 ± 425	−4.2 ± 2.1	−0.15 ± 0.08	−4.7 ± 3.0
			1	832 ± 558	−3.6 ± 1.3	−0.04 ± 0.47	−4.5 ± 1.7
Sn	4.42	231	0.1	288 ± 164	−6.4 ± 1.2	−0.09 ± 0.06	−8.1 ± 1.6
			0.5	1793 ± 288	−7.2 ± 1.4	−0.19 ± 0.09	−9.0 ± 2.5
			1	1649 ± 422	−6.4 ± 0.7	−0.11 ± 0.06	−8.0 ± 1.5
			2	1582 ± 215	−6.7 ± 0.3	−0.08 ± 0.04	−8.4 ± 1.1
Ni	5.04–5.35	1453	0.5	−128 ± 73	1.7 ± 0.7	1.2 ± 0.8	2.2 ± 0.8
			1	−435 ± 276	7.8 ± 8.2	7.5 ± 8.9	4.6 ± 11.7
Pt	5.64–5.93	1768	0.1	−584 ± 191	7.0 ± 3.5	7.5 ± 4.1	6.3 ± 4.5
			0.5	−496 ± 337	14.9 ± 7.3	20.5 ± 17.9	18.4 ± 9.1

© 2021 Wiley-VCH GmbH

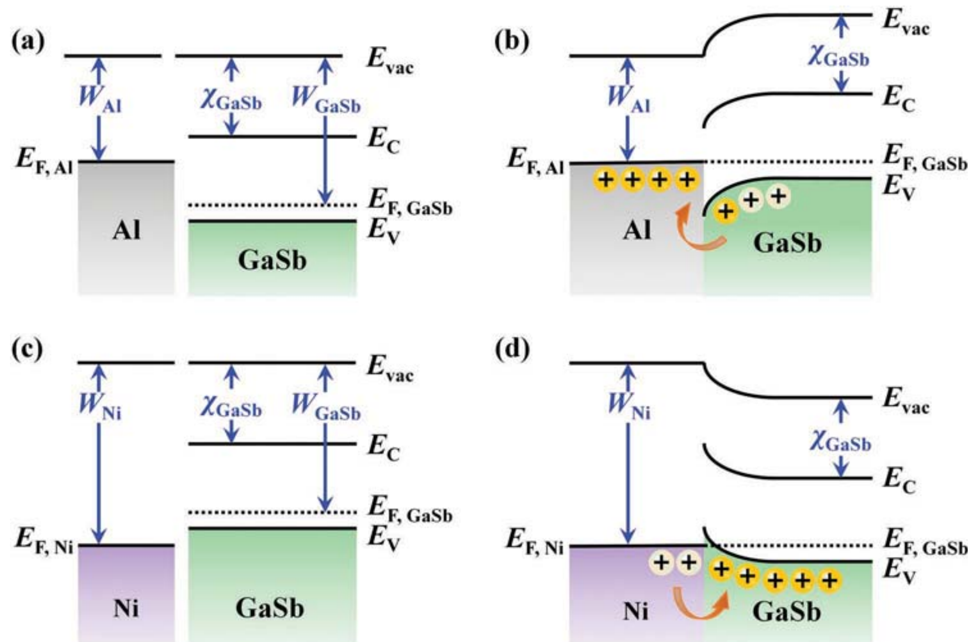

Figure 3. Schematics of unusual-high hole mobility of p-channel FETs by metal-semiconductor junctions. a,b) Energy band diagrams of low work function metal of Al and GaSb before and after constructing metal-semiconductor junctions; c,d) Energy band diagrams of high work function metal of Ni and GaSb before and after constructing metal-semiconductor junctions.

V_{TH}, the decrease/increase of hole concentration and increase/decrease of hole mobility are all in gradual. There are some values deviations observed in the case of Ti- and Sn-deposited FETs, possibly caused by the difficulty of thickness control during the deposition process. Anyway, by adopting metal-semiconductor junctions, the hole mobility of p-FETs can be enhanced efficiently.

To find out the regulation mechanism of carrier mobility, energy band diagrams of metal-semiconductor junctions are studied in detail in **Figure 3** by taking Al-GaSb junction and Ni-GaSb junction as examples. As shown in Figure 3a,c, GaSb has an energy band gap of 0.726 eV, electron affinity (χ_{GaSb}) of 4.06 eV, and work function (W_{GaSb}) of 4.76 eV, while Al has a lower work function (W_{Al}) of 4.06–4.26 eV and Ni has higher work function (W_{Ni}) of 5.04–5.35 eV. Owing to the relatively high free hole concentration, the Fermi level (E_F) of as-studied GaSb lies near the valence band edge at equilibrium. When Al film is deposited on the surface of GaSb to construct Al-GaSb junctions, as illustrated in Figure 3b, the equilibrium band diagram disturbs locally to induce a downward band-bending at Al-GaSb interface, such that the free hole flow from GaSb into Al, causing the decrease of hole concentration and the enhancement of hole mobility. On the contrary, when the metal with a higher work function, such as Ni, is deposited on the surface of GaSb to construct the Ni-GaSb junctions, the positive work function difference ($W_{Ni} - W_{GaSb}$) leads to an upward band-bending at Ni-GaSb interface, as shown in Figure 3d. In this case, the free hole transfer from Ni to GaSb, resulting in the increase of hole concentration and decrease of hole mobility. These kinds of band-bending and electrons transfer process always occur as soon as the semiconductors contact with metals, resulting from the work function difference ($W_{metal} - W_{GaSb}$). In a word, all these theoretically demonstrate the simply constructed metal-semiconductor junction here is really an efficient strategy of hole mobility enhancement.

To further demonstrate the generality of this hole mobility enhancement strategy by simply constructing metal-semiconductor junction, p-channel FETs of GaAs NW, GaAs film, and 2D WSe_2 FETs are employed in **Figure 4**. Owing to the work functions of GaAs and WSe_2 are 4.71 and 4.6–4.79 eV,[58–60] respectively, Al can be adopted as the low work function metal to construct the metal-semiconductor junctions for improving the hole mobilities. The insets of Figure 4 show the corresponding optical images of as-fabricated GaAs NW, GaAs film, and 2D WSe_2 FETs. Figure 4a shows the transfer characteristics in linear coordinates of GaAs NWFET before and after the deposition of 1 nm Al film. Obviously, after the deposition of Al film, I_{on} effectively increases from 11 to 17 pA, and V_{TH} shifts negatively. Meanwhile, the calculated $|g_m|$ of GaAs NWFET increases from 8.6 to 14.9 pS, as shown in Figure 4b, demonstrating the success in hole mobility enhancement. Besides the NW device, this hole mobility enhancement strategy is also verified in GaAs thin-film devices. Figures 4c,d illustrate the transfer characteristics and $|g_m|$ of the GaAs thin-film FET before and after the deposition of 1 nm Al film. Similarly, after constructing Al-GaAs junctions, I_{on} increases from 2.9 to 4.9 nA, and $|g_m|$ increases from 0.6 to 1.4 nS, which demonstrates more than twice the increase of hole mobility. In fact, p-type GaSb wafers are also adopted to construct the metal-semiconductor junctions for demonstrating the generality of the hole mobility enhancement strategy. As shown in Figure S5, Supporting Information, compared with that of original GaSb wafer, Hall mobility (μ_{Hall}) of the Sn-deposited GaSb wafer increases, on the other hand, μ_{Hall} of Ni-deposited GaSb wafer decreases. The variation

 © 2021 Wiley-VCH GmbH

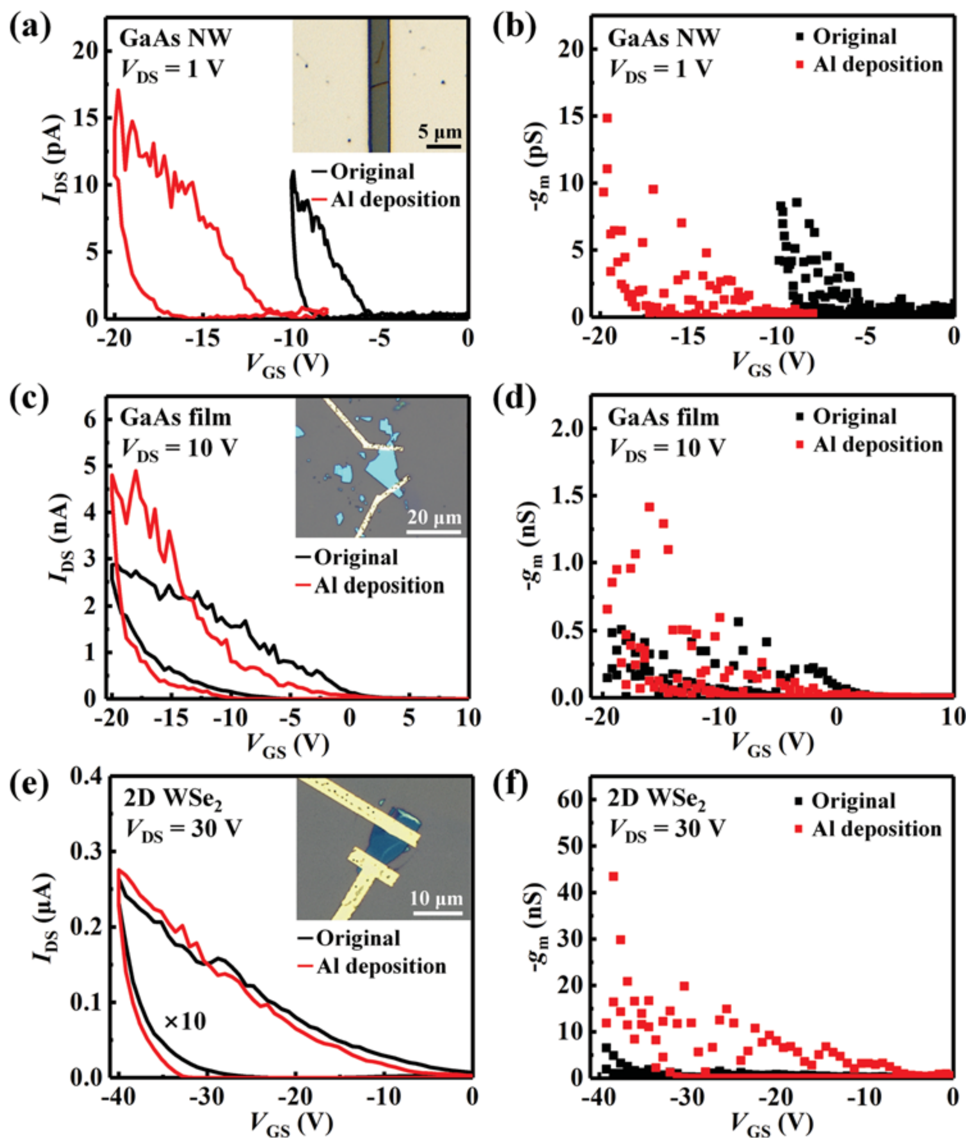

Figure 4. Generality of unusual-high hole mobility of p-channel FETs by metal-semiconductor junctions. Transfer characteristics and transconductances of a,b) GaAs NW, c,d) GaAs film, and e,f) 2D WSe_2 FETs before and after the deposition of 1 nm Al films. Insets show the corresponding optical images of as-fabricated FETs.

trends of hole concentration and μ_{Hall} are in agreement with the metal-semiconductor junctions mechanism discussed above. However, compared to NW and thin-film FETs, the hole mobility regulation of metal-deposited GaSb wafer is weak, probably attributing to the thick thickness of GaSb wafers. In this case, 2D WSe_2 with atomic scale thickness is studied in Figures 4e,f. After the deposition of 1 nm Al film, I_{on} of 2D WSe_2 FET increases from 0.03 to 0.28 μA, and $|g_m|$ increases from 6.5 to 43.5 nS, proving a six to seven times increase of hole mobility. Obviously, this metal-semiconductor junction is more efficient for atomic scale 2D semiconductors than NWs, thin film, and wafer, which is mainly because the thickness of 2D material is the thinnest and the carriers are easiest to be controlled. However, the hysteresis is still large even with the metal coverage, some strategies can be employed to eliminate or reduce the acceptable levels. Interface engineering provides an effective and promising approach to reduce hysteresis in transistor. By treating the semiconductor/dielectric interfaces with plasma ozone and self-assembled monolayer (Octadecyltrichlorosilane, octadecylphosphonic acids, hexamethyldisilazane, and the like) can effectively improve the smoothness and surface energies, thus reducing the hysteresis.[61] In brief, all the results demonstrate the simply constructed metal-semiconductor junction here is an efficient strategy for hole mobility enhancement.

After achieving unusual-high hole mobility, negative shifted V_{TH}, decreased *SS*, and remained I_{on}/I_{off}, Al-GaSb NWFET is constructed with n-type InGaAs NWFET to demonstrate the potential application in CMOS inverter. **Figure 5a** shows the transfer characteristics of the driver (GaSb NWFET deposited with 0.5 nm Al film) and the load (InGaAs NWFET) at V_{DS} = 0.1 V. V_{TH} of Al-GaSb NWFET is between 1.2 and

 © 2021 Wiley-VCH GmbH

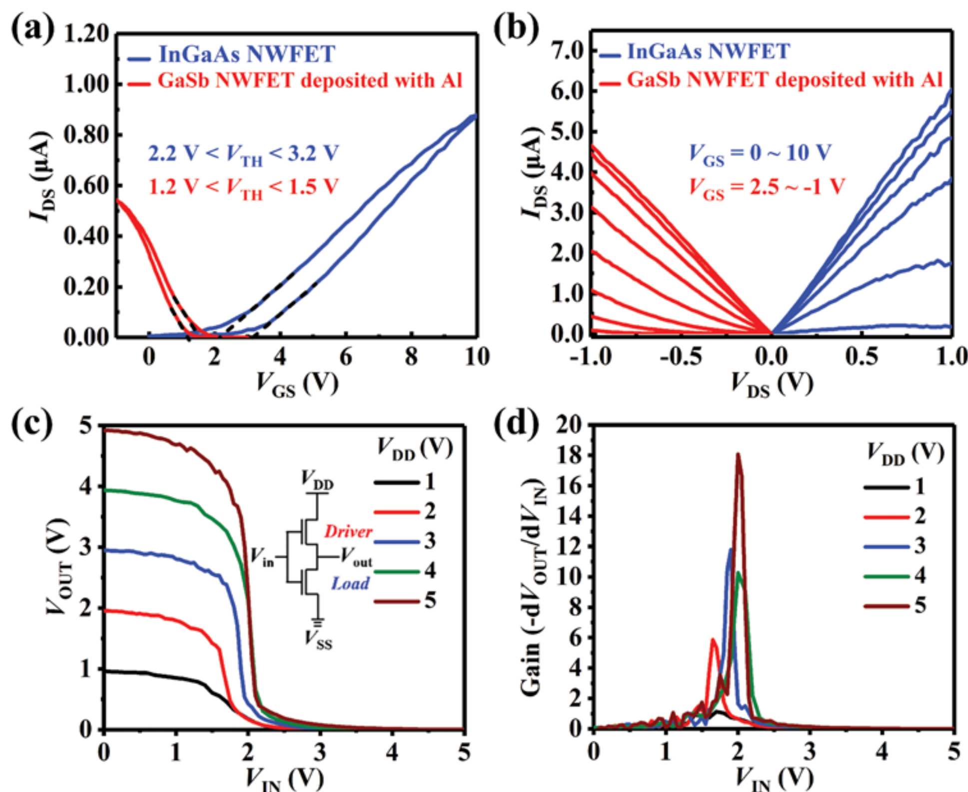

Figure 5. CMOS inverter constructed by the obtained unusual-high hole mobility GaSb NWFETs. a,b) Transfer and output characteristics of the driver (GaSb NWFET deposited with 0.5 nm Al film) and the load (InGaAs NWFET); c) the voltage transfer characteristics (VTC) of the as-fabricated CMOS inverter at different V_{DD}. The inset shows the schematic circuit diagram of the inverter; d) the voltage gain extracted by differentiating VTC.

1.5 V, and V_{TH} of InGaAs NWFET is between 2.2 and 3.2 V. V_{TH} separation between n- and p-type FETs is important in CMOS invert, ensuring the driver and load do not open at the same time. In this case, there is no direct path exists between the supply and ground rails under steady-state operating conditions, resulting in the lower power dissipation.[62] The output characteristics of driver and load are shown in Figure 5b, indicating the ohmic contact and symmetric performance of both n- and p-type FETs. The uniform and symmetric performance of p- and n-type FETs will benefit to the obtain of high-performance CMOS invert.[62] As shown in the voltage transfer characteristics (VTC) of the CMOS inverter of Figure 5c, it is obvious that the inverter can efficiently alter the logic "0" (low V_{IN}) into the logic "1" (high V_{OUT}) and vice versa under V_{DD} of 1–5 V when V_{IN} swings from 0 to 5 V. The schematic circuit diagram of the inverter is shown in the inset of Figure 5c. It is also worth noting that the inverter can function at a relatively low voltage of ≈2.5 V, along with the insignificant leakage current and reduced power consumption. In the end, benefiting from the matched mobility and separated V_{TH} between n- and p-FETs, the input signal is inverted with a relatively high gain of ≈18.1 for V_{DD} = 5 V and the CMOS inverter exhibits good time-resolved property at 100 Hz frequency under V_{DD} = 8 V (Figure 5d and Figure S6, Supporting Information), which is comparable to previous reports.[63] Further performance enhancements of CMOS invert can be achieved by optimizing device geometry for reducing the parasitic capacitance and so on.

3. Conclusion

In conclusion, metal-semiconductor junction constructed by depositing CMOS-compatible metals with lower work function has been demonstrated as an efficient strategy of hole mobility enhancement for p-channel building block device, owing to the downward band-bending at the metal-semiconductor interface and the reduced hole concentration by the injection of electrons from deposited metals. The peak hole mobility of as-studied GaSb NWFET can be enhanced as high as 3372 cm^2 V^{-1} s^{-1} after constructing Al-GaSb junctions, showing three times value than the original NWFET, which is the highest values among p-channel FETs in the atmosphere. This hole mobility enhancement strategy is generalized and can also modify the hole mobility of other p-channel devices, such as GaAs NWFET, GaAs film FET, and 2D WSe_2 FET. Constructed by the unusual-high hole mobility Al-GaSb NWFET, the as-fabricated CMOS inverter exhibits good invert characteristics with a relatively high gain of ≈18.1. The reported metal-semiconductor junctions here can be regarded as important advances in the high hole mobility p-channel building block devices and promotes the development of next-generation electronics.

Supporting Information

Supporting Information is available from the Wiley Online Library or from the author.

© 2021 Wiley-VCH GmbH

Acknowledgements

J.M.S. and X.M.Z. contributed equally to this work. The authors acknowledge the National Key R&D Program of China (No. 2017YFA0305500), National Natural Science Foundation of China (No. 61904096), Taishan Scholars Program of Shandong Province (No. tsqn201812006), Shandong University multidisciplinary research and innovation team of young scholars (No. 2020QNQT015), "Outstanding youth scholar and Qilu young scholar" programs of Shandong University, and the Youth Interdisciplinary Science and Innovative Research Groups of Shandong University.

Conflict of Interest

The authors declare no conflict of interest.

Data Availability Statement

The data that support the findings of this study are available from the corresponding author upon reasonable request.

Keywords

carrier concentration control, field-effect-transistors, GaSb nanowires, hole mobility, metal-semiconductor junction

Received: April 20, 2021
Revised: June 27, 2021
Published online:

[1] J. A. del Alamo, *Nature* **2011**, *479*, 317.
[2] K. Myny, *Nat. Electron.* **2018**, *1*, 30.
[3] X. Yuan, D. Pan, Y. Zhou, X. Zhang, K. Peng, B. Zhao, M. Deng, J. He, H. H. Tan, C. Jagadish, *Appl. Phys. Rev.* **2021**, *8*, 021302.
[4] D.-H. Park, Y. J. Cho, J.-H. Lee, I. Choi, S. H. Jhang, H.-J. Chung, *Nanotechnology* **2019**, *30*, 394003.
[5] F. Li, S. Yip, R. Dong, Z. Zhou, C. Lan, X. Liang, D. Li, Y. Meng, X. Kang, J. C. Ho, *Nano Res.* **2019**, *12*, 1796.
[6] Z. Wu, Z. Jiang, P. Song, P. Tian, L. Hu, R. Liu, Z. Fang, J. Kong, T.-Y. Zhang, *Small* **2019**, *15*, 1900580.
[7] Y. Xu, X. Shi, Y. Zhang, H. Zhang, Q. Zhang, Z. Huang, X. Xu, J. Guo, H. Zhang, L. Sun, Z. Zeng, A. Pan, K. Zhang, *Nat. Commun.* **2020**, *11*, 1330.
[8] J. Sun, Y. Yin, M. Han, Z.-x. Yang, C. Lan, L. Liu, Y. Wang, N. Han, L. Shen, X. Wu, J. C. Ho, *ACS Nano* **2018**, *12*, 10410.
[9] Y. Zhao, J. Qiao, Z. Yu, P. Yu, K. Xu, S. P. Lau, W. Zhou, Z. Liu, X. Wang, W. Ji, Y. Chai, *Adv. Mater.* **2017**, *29*, 1604230.
[10] W. Feng, W. Zheng, W. Cao, P. Hu, *Adv. Mater.* **2014**, *26*, 6587.
[11] A. N. Rudenko, S. Brener, M. I. Katsnelson, *Phys. Rev. Lett.* **2016**, *116*, 246401.
[12] J. Wu, C. Qiu, H. Fu, S. Chen, C. Zhang, Z. Dou, C. Tan, T. Tu, T. Li, Y. Zhang, Z. Zhang, L.-M. Peng, P. Gao, B. Yan, H. Peng, *Nano Lett.* **2019**, *19*, 197.
[13] R. Dingle, H. L. Stormer, A. C. Gossard, W. Wiegmann, *Appl. Phys. Lett.* **1978**, *33*, 665.
[14] W. Shi, S. Kahn, L. Jiang, S.-Y. Wang, H.-Z. Tsai, D. Wong, T. Taniguchi, K. Watanabe, F. Wang, M. F. Crommie, A. Zettl, *Nat. Electron.* **2020**, *3*, 99.
[15] S. M. Sze, K. K. Ng, *Physics of semiconductor devices*, John Wiley & Sons, Hoboken, NJ **2006**.
[16] J. Sun, M. Peng, Y. Zhang, L. Zhang, R. Peng, C. Miao, D. Liu, M. Han, R. Feng, Y. Ma, *Nano Lett.* **2019**, *19*, 5920.
[17] F. Wang, S. Yip, G. Dong, F. Xiu, L. Song, Z. Yang, D. Li, T. F. Hung, N. Han, J. C. Ho, *Adv. Mater. Interfaces* **2017**, *4*, 1700260.
[18] N. Han, F. Wang, J. J. Hou, S. P. Yip, H. Lin, F. Xiu, M. Fang, Z.-x. Yang, X. Shi, G. Dong, T. F. Hung, J. C. Ho, *Adv. Mater.* **2013**, *25*, 4445.
[19] S. Mubeen, M. Moskovits, *Adv. Mater.* **2011**, *23*, 2306.
[20] Y. Hirose, A. Kahn, V. Aristov, P. Soukiassian, V. Bulovic, S. R. Forrest, *Phys. Rev. B* **1996**, *54*, 13748.
[21] Z.-x. Yang, S. Yip, D. Li, N. Han, G. Dong, X. Liang, L. Shu, T. F. Hung, X. Mo, J. C. Ho, *ACS Nano* **2015**, *9*, 9268.
[22] Z.-x. Yang, L. Liu, S. Yip, D. Li, L. Shen, Z. Zhou, N. Han, T. F. Hung, E. Y. Pun, X. Wu, A. Song, J. C. Ho, *ACS Nano* **2017**, *11*, 4237.
[23] A. Liu, G. Liu, H. Zhu, H. Song, B. Shin, E. Fortunato, R. Martins, F. Shan, *Adv. Funct. Mater.* **2015**, *25*, 7180.
[24] H. Zhu, A. Liu, G. Liu, F. Shan, *Appl. Phys. Lett.* **2017**, *111*, 143501.
[25] J. A. Caraveo-Frescas, H. N. Alshareef, *Appl. Phys. Lett.* **2013**, *103*, 222103.
[26] K. J. Saji, K. Tian, M. Snure, A. Tiwari, *Adv. Electron. Mater.* **2016**, *2*, 1500453.
[27] C. W. Shih, A. Chin, C. F. Lu, W. F. Su, *Sci. Rep.* **2018**, *8*, 889.
[28] X. Guan, Z. Wang, M. K. Hota, H. N. Alshareef, T. Wu, *Adv. Electron. Mater.* **2019**, *5*, 1800538.
[29] Q. Cao, Y.-W. Dai, J. Xu, L. Chen, H. Zhu, Q.-Q. Sun, D. W. Zhang, *ACS Appl. Mater. Interfaces* **2017**, *9*, 18215.
[30] B. Tang, Z. G. Yu, L. Huang, J. Chai, S. L. Wong, J. Deng, W. Yang, H. Gong, S. Wang, K.-W. Ang, Y.-W. Zhang, D. Chi, *ACS Nano* **2018**, *12*, 2506.
[31] H. Chen, Y. Cao, J. Zhang, C. Zhou, *Nat. Commun.* **2014**, *5*, 4097.
[32] B. Chen, P. Zhang, L. Ding, J. Han, S. Qiu, Q. Li, Z. Zhang, L.-M. Peng, *Nano Lett.* **2016**, *16*, 5120.
[33] J. M. Salazar-Rios, A. A. Sengrian, W. Talsma, H. Duim, M. Abdu-Aguye, S. Jung, N. Froehlich, S. Allard, U. Scherf, M. A. Loi, *Adv. Electron. Mater.* **2020**, *6*, 1900789.
[34] F. Shan, A. Liu, H. Zhu, W. Kong, J. Liu, B. Shin, E. Fortunato, R. Martins, G. Liu, *J. Mater. Chem. C* **2016**, *4*, 9438.
[35] C. Zhao, C. Tan, D.-H. Lien, X. Song, M. Amani, M. Hettick, H. Y. Y. Nyein, Z. Yuan, L. Li, M. C. Scott, A. Javey, *Nat. Nanotechnol.* **2020**, *15*, 53.
[36] A. Pezeshki, S. H. H. Shokouh, P. J. Jeon, I. Shackery, J. S. Kim, I.-K. Oh, S. C. Jun, H. Kim, S. Im, *ACS Nano* **2016**, *10*, 1118.
[37] D. Qu, X. Liu, M. Huang, C. Lee, F. Ahmed, H. Kim, R. S. Ruoff, J. Hone, W. J. Yoo, *Adv. Mater.* **2017**, *29*, 1606433.
[38] E. Wu, Y. Xie, J. Zhang, H. Zhang, X. Hu, J. Liu, C. Zhou, D. Zhang, *Sci. Adv.* **2019**, *5*, eaav3430.
[39] X. Liu, D. Qu, J. Ryu, F. Ahmed, Z. Yang, D. Lee, W. J. Yoo, *Adv. Mater.* **2016**, *28*, 2345.
[40] S.-W. Min, M. Yoon, S. J. Yang, K. R. Ko, S. Im, *ACS Appl. Mater. Interfaces* **2018**, *10*, 4206.
[41] J. Guo, Y. Liu, Y. Ma, E. Zhu, S. Lee, Z. Lu, Z. Zhao, C. Xu, S.-J. Lee, H. Wu, K. Kovnir, Y. Huang, X. Duan, *Adv. Mater.* **2018**, *30*, 1705934.
[42] P. M. Campbell, A. Tarasov, C. A. Joiner, M.-Y. Tsai, G. Pavlidis, S. Graham, W. J. Ready, E. M. Vogel, *Nanoscale* **2016**, *8*, 2268.
[43] P. R. Pudasaini, A. Oyedele, C. Zhang, M. G. Stanford, N. Cross, A. T. Wong, A. N. Hoffman, K. Xiao, G. Duscher, D. G. Mandrus, T. Z. Ward, P. D. Rack, *Nano Res.* **2018**, *11*, 722.
[44] R. Tu, L. Zhang, Y. Nishi, H. Dai, *Nano Lett.* **2007**, *7*, 1561.
[45] M. Simanullang, G. B. M. Wisna, K. Usami, W. Cao, Y. Kawano, K. Banerjee, S. Oda, *J. Mater. Chem. C* **2016**, *4*, 5102.
[46] Y. Li, R. Zhang, *Appl. Phys. Lett.* **2019**, *114*, 132101.
[47] Z.-x. Yang, N. Han, F. Wang, H.-Y. Cheung, X. Shi, S. Yip, T. Hung, M. H. Lee, C.-Y. Wong, J. C. Ho, *Nanoscale* **2013**, *5*, 9671.
[48] L. Li, Y. Yu, G. J. Ye, Q. Ge, X. Ou, H. Wu, D. Feng, X. H. Chen, Y. Zhang, *Nat. Nanotechnol.* **2014**, *9*, 372.

 © 2021 Wiley-VCH GmbH

[49] W. C. Tan, Y. Cai, R. J. Ng, L. Huang, X. Feng, G. Zhang, Y.-W. Zhang, C. A. Nijhuis, X. Liu, K.-W. Ang, *Adv. Mater.* **2017**, *29*, 1700503.
[50] X. Feng, X. Huang, L. Chen, W. C. Tan, L. Wang, K.-W. Ang, *Adv. Funct. Mater.* **2018**, *28*, 1801524.
[51] D. He, Y. Wang, Y. Huang, Y. Shi, X. Wang, X. Duan, *Nano Lett.* **2019**, *19*, 331.
[52] Z.-x. Yang, F. Wang, N. Han, H. Lin, H. Y. Cheung, M. Fang, S. Yip, T. Hung, C. Y. Wong, J. C. Ho, *ACS Appl. Mater. Interfaces* **2013**, *5*, 10946.
[53] Z.-x. Yang, N. Han, M. Fang, H. Lin, H. Y. Cheung, S. Yip, E. J. Wang, T. Hung, C. Y. Wong, J. C. Ho, *Nat. Commun.* **2014**, *5*, 5249.
[54] M. Yokoyama, H. Yokoyama, M. Takenaka, S. Takagi, *Appl. Phys. Lett.* **2015**, *106*, 073503.
[55] G. Long, D. Maryenko, J. Shen, S. Xu, J. Hou, Z. Wu, W. K. Wong, T. Han, J. Lin, Y. Cai, R. Lortz, N. Wang, *Nano Lett.* **2016**, *16*, 7768.
[56] C. Lan, S. Yip, X. Kang, Y. Meng, X. Bu, J. C. Ho, *ACS Appl. Mater. Interfaces* **2020**, *12*, 56330.
[57] X. Zhuang, W. Huang, S. Han, Y. Jiang, H. Zheng, J. Yu, *Org. Electron.* **2017**, *49*, 334.
[58] G. W. Gobeli, F. G. Allen, *Phys. Rev.* **1965**, *137*, A245.
[59] S. Seo, S. Kim, H. Choi, J. Lee, H. Yoon, G. Piao, J.-C. Park, Y. Jung, J. Song, S. Y. Jeong, H. Park, S. Lee, *Adv. Sci.* **2019**, *6*, 1900301.
[60] T. Guo, C. Ling, T. Zhang, H. Li, X. Li, X. Chang, L. Zhu, L. Zhao, Q. Xue, *J. Mater. Chem. C* **2018**, *6*, 5821.
[61] H. Chen, W. Zhang, M. Li, G. He, X. Guo, *Chem. Rev.* **2020**, *120*, 2879.
[62] Z. Zhang, S. Wang, Z. Wang, L. Ding, T. Pei, Z. Hu, X. Liang, Q. Chen, Y. Li, L.-M. Peng, *ACS Nano* **2009**, *3*, 3781.
[63] A. W. Dey, J. Svensson, B. M. Borg, M. Ek, L.-E. Wernersson, *Nano Lett.* **2012**, *12*, 5593.

© 2021 Wiley-VCH GmbH